Article

Cell Stem Cell

dsRNA Released by Tissue Damage Activates TLR3 to Drive Skin Regeneration

Graphical Abstract

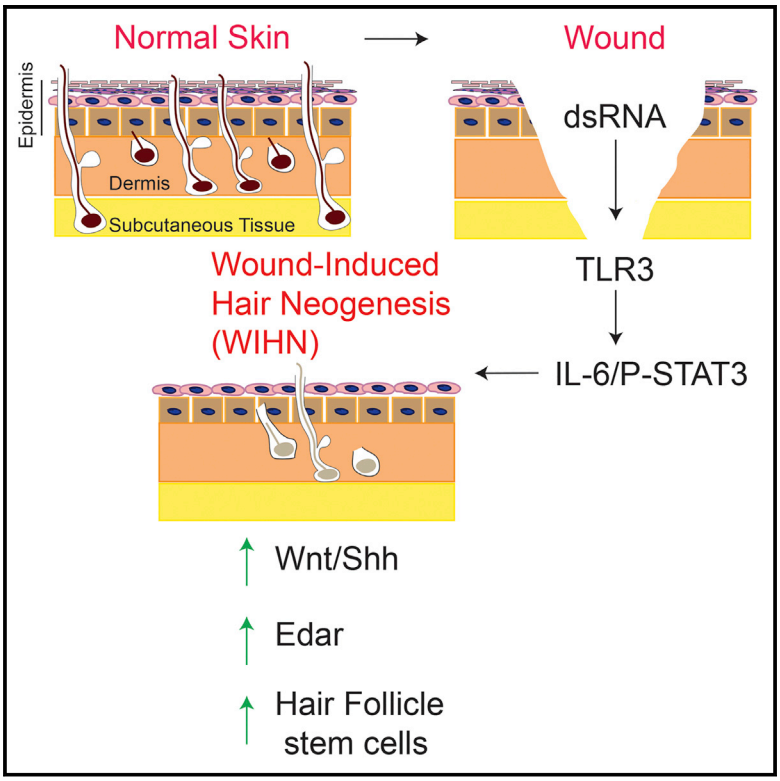

Highlights

- dsRNA released after skin injury triggers skin regeneration via TLR3
- IL-6 and Stat3 signaling, downstream mediators of TLR3, are key to regeneration
- Loss of TLR3, IL-6Ra, or Stat3 reduces hair neogenesis after wounding
- TLR3 induces core hair morphogenetic programs and hair follicle markers

Authors

Amanda M. Nelson, Sashank K. Reddy, Tabetha S. Ratliff, ..., Alexander J. Whittam, Lloyd S. Miller, Luis A. Garza

Correspondence

lag@jhmi.edu

In Brief

Wound-induced hair neogenesis provides a model for deciphering the mechanisms underlying mammalian regeneration. Nelson et al. show that dsRNA released from damaged skin triggers TLR3 activation and the downstream effector pathways IL-6/Stat3, leading to upregulation of hair follicle markers and activation of core hair morphogenetic programs.

Nelson et al., 2015, Cell Stem Cell *17*, 1–13
August 6, 2015
http://dx.doi.org/10.1016/j.stem.2015.07.008

CellPress

Please cite this article in press as: Nelson et al., dsRNA Released by Tissue Damage Activates TLR3 to Drive Skin Regeneration, Cell Stem Cell (2015), http://dx.doi.org/10.1016/j.stem.2015.07.008

Cell Stem Cell
Article

dsRNA Released by Tissue Damage Activates TLR3 to Drive Skin Regeneration

Amanda M. Nelson,[1,3,4] Sashank K. Reddy,[2,3] Tabetha S. Ratliff,[1] M. Zulfiquer Hossain,[1] Adiya S. Katseff,[1] Amadeus S. Zhu,[1] Emily Chang,[1] Sydney R. Resnik,[1] Carly Page,[1] Dongwon Kim,[1] Alexander J. Whittam,[1] Lloyd S. Miller,[1] and Luis A. Garza[1,*]
[1]Department of Dermatology
[2]Department of Plastic Surgery
Johns Hopkins University School of Medicine, Baltimore, MD 21231, USA
[3]Co-first author
[4]Present Address: Department of Dermatology, Penn State Hershey, Hershey, PA 17033, USA
*Correspondence: lag@jhmi.edu
http://dx.doi.org/10.1016/j.stem.2015.07.008

SUMMARY

Regeneration of skin and hair follicles after wounding—a process known as wound-induced hair neogenesis (WIHN)—is a rare example of adult organogenesis in mammals. As such, WIHN provides a unique model system for deciphering mechanisms underlying mammalian regeneration. Here, we show that dsRNA, which is released from damaged skin, activates Toll-Like Receptor 3 (TLR3) and its downstream effectors IL-6 and STAT3 to promote hair follicle regeneration. Conversely, TLR3-deficient animals fail to initiate WIHN. TLR3 activation promotes expression of hair follicle stem cell markers and induces elements of the core hair morphogenetic program, including ectodysplasin A receptor (EDAR) and the Wnt and Shh pathways. Our results therefore show that dsRNA and TLR3 link the earliest events of mammalian skin wounding to regeneration and suggest potential therapeutic approaches for promoting hair neogenesis.

INTRODUCTION

Animals across diverse phyla can regenerate lost structures, a capacity that is considerably more limited in mammals. Several chordate species, including urodele salamanders and teleost fish, can regenerate appendages and solid organs, yet among mammals such adult organogenesis is rarely, if ever, observed. An important exception is wound-induced hair neogenesis (WIHN), a phenomenon in which skin, sebaceous glands, and hair follicles are regenerated following large, full-thickness wounds in mice or rabbits (Breedis, 1954; Ito et al., 2007). The complete regeneration observed in WIHN is in marked contrast to the fibrotic scarring that typically results from cutaneous wound healing. Regenerated hair follicles are complex mini-organs with disparate cell types, dedicated neurovascular support, and a distinct stem cell compartment located in the bulge region. These stem cells not only repopulate hair follicles throughout life, but also aid in skin re-epithelialization after wounding, pointing to the potential therapeutic relevance of WIHN (Ito et al., 2007). As WIHN represents a rare example of adult organogenesis in mammals, understanding its mechanisms could aid in efforts to regenerate other structures.

While originally described in the 1940s, WIHN has recently been characterized in morphogenetic and molecular detail (Breedis, 1954; Gay et al., 2013; Ito et al., 2007; Kligman and Strauss, 1956; Myung et al., 2013; Nelson et al., 2013). Following complete excision of skin down to fascia, wounds on the backs of mice heal through initial contracture and then re-epithelialization. Subsequently, hair follicle morphogenesis ensues with recapitulation of events that occur during embryonic hair development. Formation and invagination of epithelial placodes in the epidermis, induction of adjacent dermal papillae, and ultimately, elaboration of distinct hair cell subtypes are observed (Ito et al., 2007). Follicle-associated structures such as sebaceous glands are also regenerated. Regenerated follicles transit through multiple hair cycles, just like neighboring hairs from unwounded skin (Ito et al., 2007). Therefore, WIHN represents functional regeneration rather than mere wound repair through scarring.

Developmental pathways required for embryonic organogenesis can be reactivated following trauma. In axolotl limb regeneration, for example, Shh signaling is activated at the site of injury in the residual limb, much as it is induced in the zone of polarizing activity during limb development (Torok et al., 1999). Similarly, during WIHN, signaling pathways utilized in embryonic hair formation reemerge after wounding. Activation of the canonical Wnt pathway is one of the earliest events observed in follicular morphogenesis. Wnt activation occurs around E15 in mice as the undifferentiated epithelium begins to condense into epithelial placodes at sites of future follicle formation (Millar, 2002). Similarly, after cutaneous wounding, the Wnt ligand, Wnt10b, and the Wnt effector, Lef1, are induced after re-epithelialization is complete, but prior to the emergence of new follicles (Ito et al., 2007). Wnt pathway activation is critical for hair morphogenesis during both development and regeneration, as mice deficient in Wnt signaling fail to generate hairs (Ito et al., 2007; Myung et al., 2013). Secondary to Wnt activation during follicular development, Shh signaling is induced in epithelial placodes and underlying dermal papillae. Activation of the Shh pathway contributes to subsequent hair follicle invagination and morphogenesis (St-Jacques et al., 1998). The Shh pathway is similarly induced

during adult hair follicle regeneration. Other molecular details of hair regeneration are shared with hair development, including expression of the hair cytokeratin Krt17 and activation of alkaline phosphatase activity in dermal papillae (Ito et al., 2007).

While downstream morphogenetic events in WIHN parallel those in hair development, the signals triggering reactivation of these programs in adult regeneration are unclear. To initiate regeneration, organisms must first sense a loss of tissue integrity. Candidate signals include molecules liberated from damaged tissues as well as mediators released by infiltrating immune cells. In newts and axolotls, activation of thrombin is a key early event in regeneration. For example, inhibition of thrombin activation abrogates lens regeneration in newts (Imokawa and Brockes, 2003). Recently, it was demonstrated that FGF9 released from $\gamma\delta$ T cells several days after wounding promotes hair regeneration in rodents (Gay et al., 2013). However, the most proximal signals released by damaged keratinocytes to initiate regeneration in the skin remain unknown. Discovery of such damage-associated signals may explain why wound healing during WIHN proceeds through regeneration, whereas most cutaneous wound healing in mammals leads to fibrotic scarring. Identifying these molecules may also suggest therapeutic approaches to promote skin and hair regeneration and reduce fibrosis.

To identify molecular events that initiate regeneration, we exploited the natural variation in follicle regenerative capacity observed in various mouse strains. Through gene expression screening of healed wounds prior to the onset of follicle regeneration, we identified the pattern recognition receptor, Toll-like Receptor 3 (TLR3), as a critical regulator of cutaneous regeneration. While TLR3 and its ligand, double-stranded RNA (dsRNA), are known to be active during cutaneous wounding, their role in promoting regeneration after re-epithelialization of the skin has not been appreciated (Lin et al., 2012). We identified dsRNA released from damaged cells as a key trigger of the regeneration process through its activation of TLR3. The ensuing damage-induced signaling cascade impedes stratification and maintains keratinocytes in a less differentiated state. Furthermore, TLR3 activation initiates molecular events in the hair morphogenetic program, with activation of canonical Wnt and Shh pathways, and ectodysplasin A receptor (EDAR) resulting in augmented hair follicle neogenesis. Thus, TLR3 activation by dsRNA links damage sensing after wounding to the earliest molecular events in hair regeneration. These results uncover a role for TLR3 as a master regulator of regeneration in the skin.

RESULTS

Hair follicle regeneration after wounding recapitulates embryonic follicle development in both morphogenetic and molecular detail. However, the events that dictate whether wound healing proceeds by regeneration or fibrotic scarring remain unclear. In studies characterizing molecular mechanisms of WIHN, we and others observed significant differences in the regenerative capacity of various mouse strains when visualized by confocal scanning laser microscopy (CSLM) (Figure 1A) (Fan et al., 2011; Ito et al., 2007; Nelson et al., 2013). To identify factors that may initiate regeneration, we compared gene expression profiles from healed wounds of mice with high and low regenerative capacity using C57BL/6 and our mixed background strain of mice (C57BL/6 × FVB × SJL). This analysis was performed at the time of wound closure but before the onset of hair morphogenesis to enrich for upstream factors in the WIHN pathway (Figure S1A). Ingenuity Pathway Analysis identified ''viral pattern recognition receptors'' and ''interferon-signaling'' as the most significantly upregulated pathways in highly regenerative mice.

dsRNA Released by Tissue Damage Activate TLR3 to Promote Regeneration

We focused on the pattern recognition receptor TLR3, which is activated by dsRNA and known to induce interferon signaling (Uematsu and Akira, 2007). The gene expression pattern we observed in highly regenerative murine skin wounds showed strong overlap with the pattern obtained from human keratinocytes treated with the synthetic dsRNA mimic poly (I:C) (Figure 1B) (Karim et al., 2011). Strikingly, despite the differences in species and experimental conditions, 25 of the 200 most highly upregulated genes were common to both analyses (Figure S1B). This observed overlap in expression of genes involved in dsRNA-sensing suggested a potentially conserved role for TLR3 in early wound healing responses. Furthermore, expression of *TLR3* itself was 3-fold higher in our highly regenerative mouse strain, as observed by qRT-PCR, validating the expression patterns observed in the array analyses (Figure 1C).

In previous studies, *TLR3* mRNA was induced in response to dsRNA released after UVB irradiation (Bernard et al., 2012). This suggested to us that during WIHN, TLR3 may serve as a sensor of tissue damage, consistent with an upstream role in the regeneration process. To test this idea, we examined TLR3 expression following scratching of human keratinocytes in culture. TLR3 expression was nearly 5-fold higher in scratched keratinocytes compared with unmanipulated controls (Figure 1D). Furthermore, we observed a significant increase in the number of regenerated follicles in vivo when we increased the extent of damage during wounding by placing minute perpendicular cuts at the wound edge (Figure 1E). We next explored whether augmenting the natural dsRNA release during wounding could lead to an increase in regeneration. Indeed, a single addition of the dsRNA mimic poly (I:C) into murine skin wounds led to a greater number of regenerated follicles (Figures 1F–1H). Conversely, addition of the dsRNA-specific endonuclease, RNase III, significantly decreased the number of regenerated follicles (Figure 1I). To confirm that the effects of dsRNA on WIHN are TLR3 dependent, we next examined the extent of regeneration in TLR3 null mice. Strikingly, regeneration was almost completely abolished in these mice compared with strain-matched controls, despite their comparable re-epithelialization kinetics (Figures 1J and 1C). Moreover, the stimulatory effect of dsRNA on WIHN was abrogated in TLR3 null mice, demonstrating the necessity of TLR3 for damage-induced regeneration (Figure 1K). The effects of dsRNA were only observed in the context of regeneration, as poly (I:C) did not affect the hair cycle in normal non-wounded murine skin (Figure S1D). Taken together, these data suggest that TLR3 activation by dsRNA released during wounding initiates regeneration.

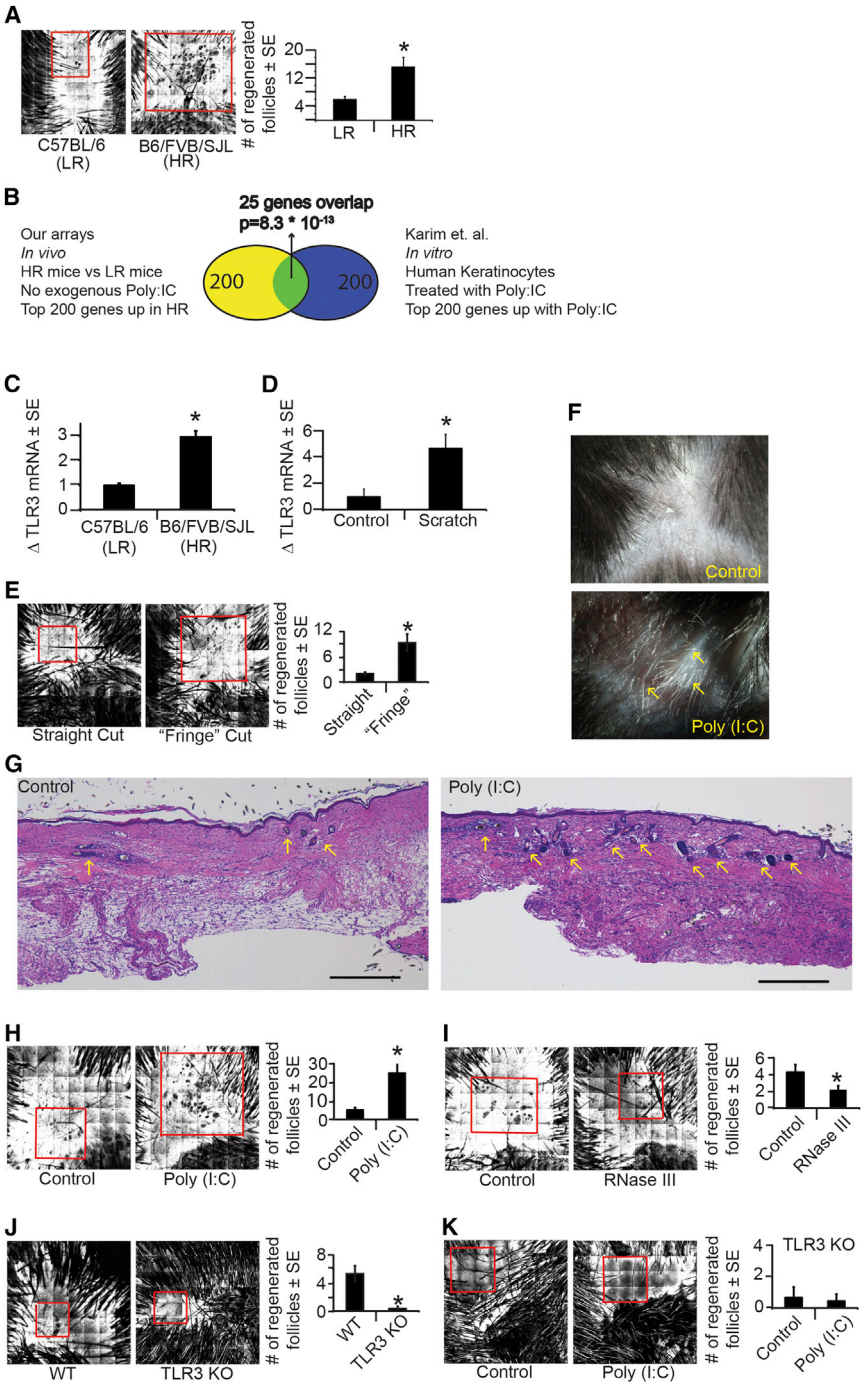

Figure 1. Tissue Damage and dsRNA activate TLR3 to Promote WIHN

(A) CSLM images for C57BL6J (low regeneration [LR]) and Mixed B6/FVB/SJL (high regeneration [HR]) strains of mice. Area of WIHN is shown within red box. Original image size is 4 mm^2.

(B) Venn diagram depicting significant overlap between genes associated with high levels of follicle regeneration in mouse skin (in vivo) and human keratinocytes treated with poly (I:C) in vitro, published by Karim et al. (2011) under GEO: GSE21260.

(C) Mean fold change in *TLR3* mRNA in healed scars at WD20-24 in LR versus HR mice, as determined by qRT-PCR and normalized to housekeeping gene β-actin.

(D) Mean fold change in *TLR3* mRNA 4 hr after scratch assay in NHEK, as determined by qRT-PCR and normalized to housekeeping gene RPLP0.

(E) WIHN levels in WT mice after standard straight cut or "fringe cut" to wound edge, n = 14–15 mice. Area of WIHN is shown within red box. Original image size is 4 mm^2.

(F) Regenerated hair shafts (white, arrows) in healed wounds after single injection of poly (I:C) (500 ng) or control at WD3 and visualized by dissecting microscope at ~WD58–62.

(G) Cross-sectional H&E histology through the middle of healed scar at WD22 after single injection of poly (I:C) as in (F). Regenerated hair follicles are marked with arrows. Scale bar represents 500 μm.

(H) WIHN levels in WT mice after poly (I:C) (500 ng) or PBS control measured by CSLM, n = 10–11 mice.

(I) WIHN levels in WT mice after RNase III (15 units) or buffer control measured by CSLM, n = 17–19 mice.

(J) WIHN levels in strain-matched WT control mice and TLR3 KO mice measured by CSLM, n = 6 mice.

(K) WIHN in TLR3 KO mice after poly (I:C) (500ng) compared with PBS control measured by CSLM, n = 9 mice.

*p < 0.05 by Student's t test or single factor ANOVA.

IL-6 and pSTAT3 Are Induced by Tissue Damage and dsRNA

To examine the mechanism by which TLR3 promotes regeneration, we performed gene expression analysis on mice at 16 to 18 days post-wounding (WD16–18), later than the array above, and at the earliest time points at which regenerated follicles can be detected by CSLM (Figure S2A). Gene expression from healed wound beds of animals with robust regeneration (average 49 hair follicles) was compared with those of animals that failed to regenerate hair follicles (zero hair follicles), revealing upregulation of several interleukins and cytokines in more highly regenerative mice. Of particular interest were interleukin-6 (IL-6) and its pathway components as well as TLR3 itself, which appeared as the top upstream regulator of IL-6 in this analysis (Figures S2B–S2F). Just as we had found for TLR3, mixed strain animals with high regenerative capacity had 3-fold higher levels of IL-6 compared with C57BL/6 mice with poor regeneration (Figure 2A). These data led to the hypothesis that IL-6 may mediate the effects of TLR3 on regeneration. TLR3 has previously been demonstrated to induce IL-6 in a dsRNA-dependent manner (Melkamu et al., 2013), and IL-6 is a known activator of regeneration in other contexts, particularly in response to liver damage (Galun and Rose-John, 2013; Jia, 2011). Consistent with this, just as TLR3 expression is increased in injured (scratched) keratinocytes in culture, *IL-6*

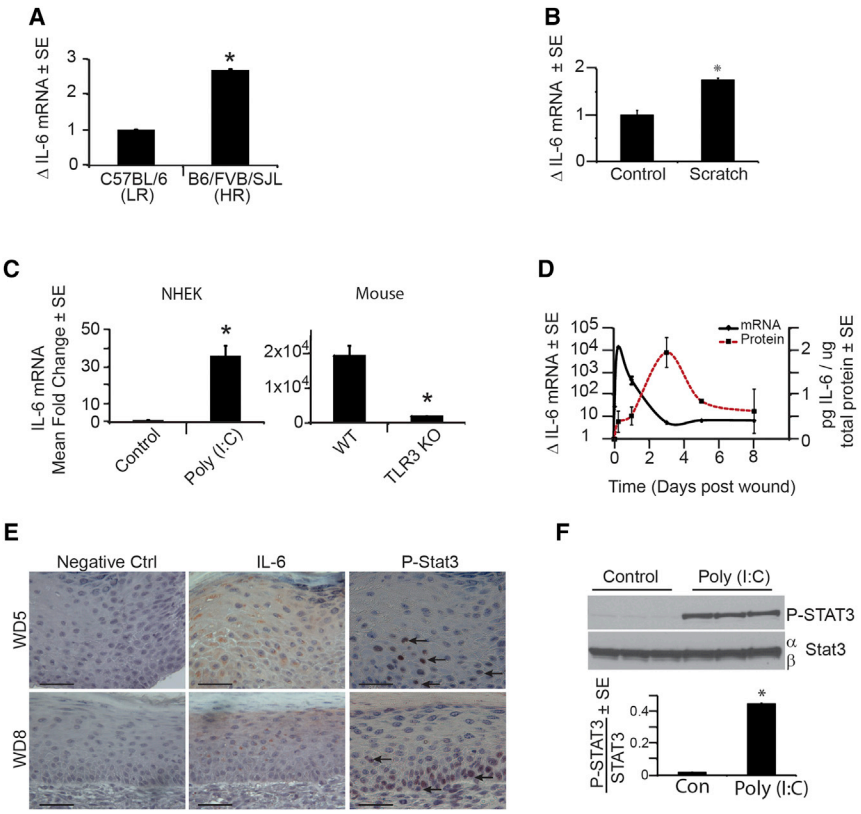

Figure 2. IL-6 and pSTAT3 Are Induced by Tissue Damage and dsRNA

(A) Mean fold change in *IL-6* mRNA in healed scars at WD20-24 in HR versus LR strains of mice, as determined by qRT-PCR and normalized to housekeeping gene β-actin.

(B) Mean fold change in *IL-6* mRNA 24 hr post scratch assay in NHEK, as determined by qRT-PCR and normalized to housekeeping gene, RPLP0.

(C) Mean fold change in *IL-6* mRNA after poly (I:C) addition (20 μg/ml) to NHEK for 6 hr or in strain-matched WT and TLR3 KO mice (n = 3) 6 hr after wounding as determined by qRT-PCR and normalized to housekeeping gene RPLP0 (NHEK) or β-actin (mouse).

(D) Time course of *IL-6* mRNA and protein expression throughout early stage wound healing in WT mice, as determined by qRT-PCR and ELISA, respectively. n = 3 mice per time point.

(E) IL-6 (middle) and P-STAT3 (right; arrows) immunohistochemistry of healing scars at WD5 (top) and WD8 (bottom) in WT mice. Scale bar represents 50 μm.

(F) P-STAT 3 levels in NHEKs after poly (I:C) (20ug/mL) for 24 hr compared with vehicle control, as measured by western blot and normalized to STAT3.

*$p < 0.05$ by Student's t test or single factor ANOVA.

mRNA also increased (Figure 2B). In keratinocytes treated with poly (I:C), we observed a greater than 30-fold induction of *IL-6* mRNA (Figure 2C), which is partially mediated through the downstream transcription factor, NF-κB (Figure S2G). This induction is TLR3 dependent, as TLR3 null animals had far less *IL-6* mRNA after wounding than strain-matched controls (Figure 2C). Temporally, *IL-6* mRNA and protein were sequentially upregulated at early time points following wounding, consistent with a role for this pathway in initiating WIHN (Figure 2D).

IL-6 receptor engagement is known to cause phosphorylation of STAT3 (pSTAT3), leading to its nuclear translocation and transcriptional activation (Heinrich et al., 2003). Consistent with a role for TLR3 and IL-6 signaling in WIHN initiation, we observed increased IL-6 and pSTAT3 protein in murine keratinocytes at WD5 and WD8 (Figures 2E and S3), as well as increased pSTAT3 protein expression in human keratinocytes following poly (I:C) treatment (Figure 2F).

TLR3 Effects on Regeneration Are Mediated by IL-6 and pSTAT3

To test the functional consequences of IL-6 on follicle regeneration, we injected recombinant IL-6 protein (rmIL-6) into mice following wounding and examined subsequent hair follicle regeneration. Compared with vehicle injected controls, mice receiving IL-6 had a nearly 3-fold increase in the number of regenerated follicles (Figures 3A–3C). The increase in follicle numbers upon activation of the IL-6/STAT3 axis occurred only in the context of WIHN, as dsRNA does not stimulate anagen onset during follicular cycling in unwounded skin (Figure S1D). We also noted a marked reduction in WIHN in mice whose keratinocytes lacked the IL-6 receptor alpha (K14CreERT2-IL-6R$\alpha^{fl/fl}$) (Figure 3D), highlighting the importance of the IL-6 signaling pathway during WIHN.

We next blocked the IL-6/STAT3 signaling axis with cucurbitacin I, a highly selective pharmacological inhibitor of STAT3 (Blaskovich et al., 2003). Cucurbitacin I strongly suppressed STAT3 phosphorylation in vivo (Figure 3E), and WT mice injected with cucurbitacin I had a greater than 3-fold decrease in the number of regenerated follicles (Figure 3F). Similarly, WIHN in keratinocyte-specific Stat3 KO mice (K5CreERT2-Stat3$^{fl/fl}$) was significantly decreased compared with control mice (Figure 3G). Remarkably, the previously observed attenuation of WIHN in TLR3 KO mice was rescued by a single injection of recombinant IL-6 protein (Figure 3H), implying that IL-6 functions downstream of TLR3 in follicle regeneration. In aggregate, these data suggest that TLR3 activation during wounding promotes IL-6 production and STAT3 phosphorylation resulting in higher regeneration.

TLR3 Activation Alters Keratinocyte Differentiation and Induces Markers of Hair Follicle Progenitors

Previous studies revealed that keratinocytes outside of the bulge region, which ordinarily differentiate into corneocytes during stratification, contribute to regenerated hair follicles during WIHN (Ito et al., 2007; Snippert et al., 2010). This finding implies that the normal stratification program is altered during hair follicle regeneration. We hypothesized that TLR3 activation during WIHN may counter stratification of keratinocytes.

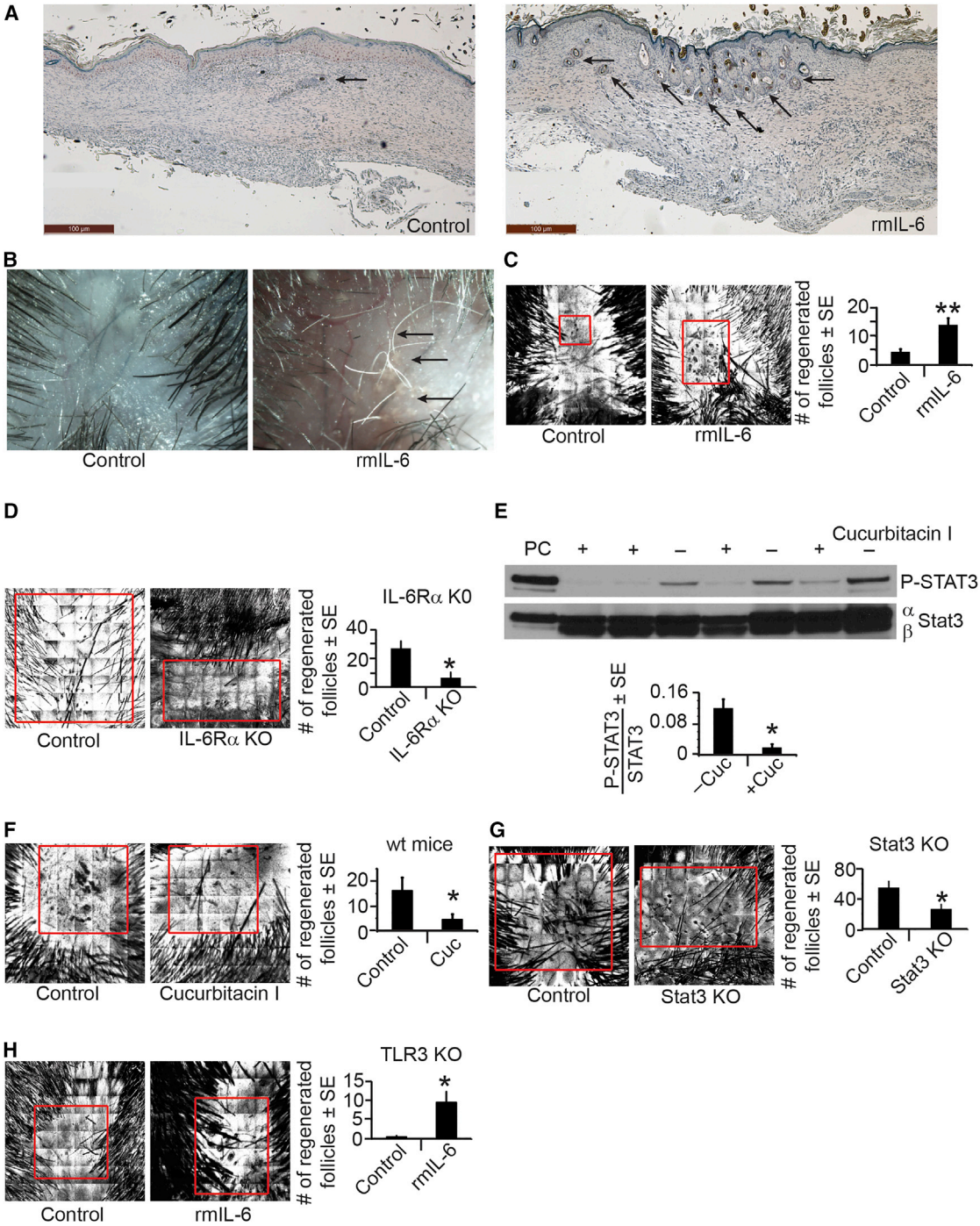

Figure 3. IL-6 and pSTAT3 Mediate TLR3 Effects on WIHN

(A) Cross-sectional H&E histology of healed scar at WD22 after a single injection of IL-6 (25 ng) or PBS control at WD7. Regenerated hair follicles are marked with arrows. Scale bar represents 100 μm.

(B) Regenerated hair shafts (white, arrows) at ~WD58–62, as visualized by dissecting microscope.

(C) WIHN in WT mice after single dose of IL-6 (25 ng) compared with PBS control, as measured by CSLM, n = 30 mice.

(D) WIHN in keratinocyte-specific knockout of IL-6Receptorα compared to control mice measured by CSLM, n = 3–6 mice.

(E) P-Stat3 levels in the presence of cucurbitacin I (+) compared to control (–) in WT mice as measured by western blot and normalized to Stat3. PC is P-STAT3-positive control cell lysate.

(F) WIHN levels in WT mice after cucurbitacin I (2mg/kg) or control, as measured by CSLM, n = 10–14 mice.

(G) WIHN in keratinocyte-specific knockout of Stat3 compared with control mice measured by CSLM, n = 10–15 mice.

(H) WIHN in TLR3 KO mice after single dose of rmIL-6 (500 ng) compared with PBS control measured by CSLM, n = 8–10 mice.

*$p < 0.05$ by Student's t test or single factor ANOVA.

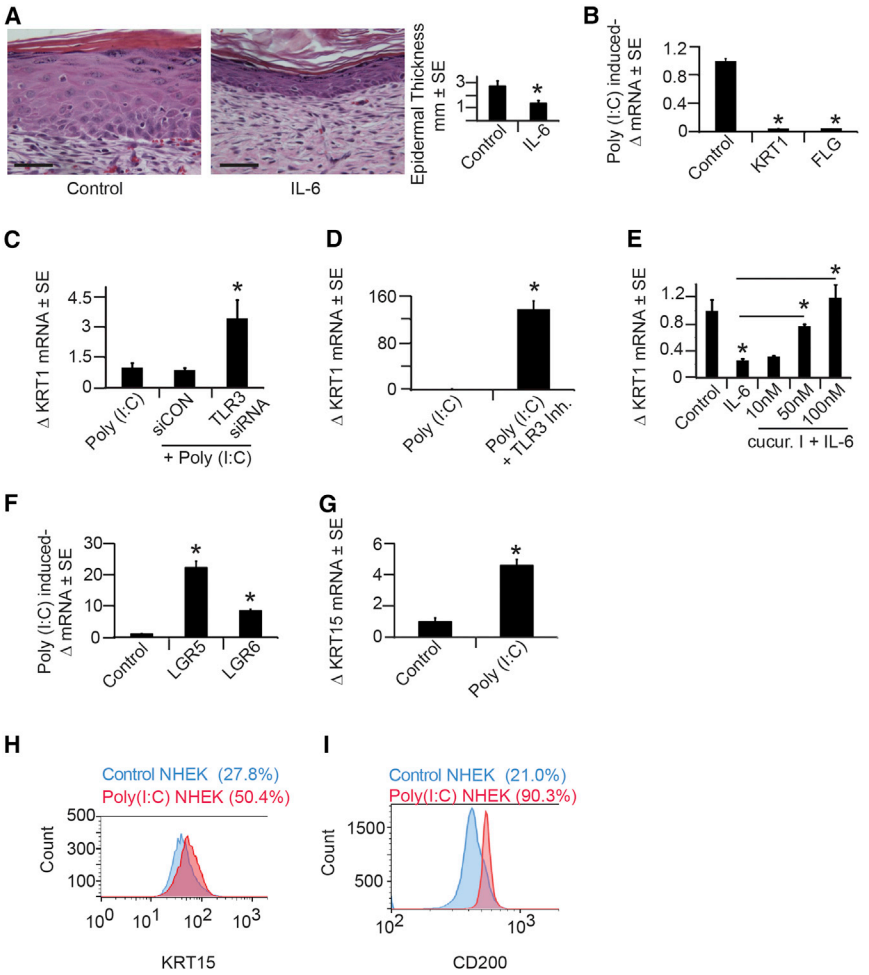

Figure 4. TLR3 Activation Alters Keratinocyte Differentiation and Induces Markers of Hair Follicle Progenitors

(A) Cross-sectional H&E histology through healed scars treated with IL-6 (25 ng) or control (PBS) at WD7. Scale bar represents 100 μm. Quantification of healed epidermal thickness in healed scars after control or IL-6 addition is shown.

(B) Mean fold change in *KRT1* and *FLG* mRNA after poly (I:C) (20 μg/ml) addition to NHEK for 24 hr as determined by qRT-PCR and normalized to housekeeping gene, RPLP0.

(C) Mean fold change in *KRT1* mRNA with TLR3-specific or scrambled control siRNA in the presence of poly (I:C) (20 μg/ml) in NHEK as determined by qRT-PCR and normalized as in (B).

(D) Mean fold change in *KRT1* mRNA with TLR3-specific inhibitor or control in the presence of poly (I:C) (20 μg/ml) in NHEK as determined by qRT-PCR and normalized as in (B).

(E) Mean fold change in *KRT1* mRNA after IL-6 (50 ng/ml) +/− cucurbitacin I in NHEK for 24 hr as determined by qRT-PCR and normalized as in (B).

(F) Mean fold change in Wnt pathway genes, *Lgr5* and *Lgr6*, mRNA after 6 days of continuous exposure to poly (I:C) determined by qRT-PCR and normalized to housekeeping gene, RPLP0.

(G) Mean fold change in *KRT15* mRNA 72 hr after 24 hr of poly (I:C) (20 μg/ml) treatment to NHEK as determined by qRT-PCR normalized to housekeeping gene, RPLP0.

(H) Flow cytometry analysis of KRT15 protein expression of NHEKs treated as in (G).

(I) Flow cytometry analysis of CD200 protein expression of NHEKs treated as in (G).

*$p < 0.05$ by Student's t test or single factor ANOVA.

To test this idea, we first injected mice with IL-6 and assessed epidermal thickness as an index of stratification. Ordinarily, stratification causes thickening of the epidermis due to the accumulation of differentiated keratinocytes. However, mice treated with IL-6 had a 2-fold reduction in epidermal thickness compared with strain-matched controls, implying decreased stratification (Figure 4A) because no alterations in apoptosis or proliferation were observed with IL-6 treatment (Figure S4A). Consistent with our findings in vivo, direct TLR3 activation with poly (I:C) in cultured keratinocytes led to a nearly complete loss of expression of markers of keratinocyte differentiation such as keratin 1 (KRT1) and filaggrin (FLG) (Figure 4B). This effect was TLR3 dependent as inhibition of TLR3 through siRNA-mediated depletion or direct small molecule-based antagonism abrogated the loss of KRT1 (Figures 4C, 4D, and S4B). Similarly, keratinocytes treated with IL-6 had a profound decrease in KRT1 expression, an effect that was reversed by the addition of cucurbitacin I (Figure 4E). These data suggest that induction of the TLR3/IL-6 axis during wounding prevents keratinocyte differentiation. Interestingly, the morphology of poly (I:C)-treated keratinocytes was also altered and came to resemble that of keratinocytes in healing human skin wounds (Figure S4C–S4H) (Yan et al., 2010).

We next examined whether in response to TLR3 activation keratinocytes adopt a less differentiated state that is permissive for subsequent hair follicle differentiation. Following treatment with poly (I:C), keratinocytes expressed markers associated with hair progenitors, including leucine-rich-repeat containing G proteins (LGR) 5 and 6 (Figure 4F) (Tadeu and Horsley, 2014). Induction of LGR6 is particularly notable, as previous lineage tracing experiments demonstrated that LGR6 expressing cells contribute to regenerating hair follicles during WIHN (Snippert et al., 2010). Further, we noticed induction of genes associated with hair follicle stem cells upon TLR3 activation. Hair follicle stem cells reside in the bulge region of the follicle and express keratin 15 (KRT15), which is considered the most reliable marker of this population (Liu et al., 2003), and CD200, which is associated with hair follicle progenitor cells (Garza et al., 2011). We found significantly increased expression of *KRT15* mRNA in keratinocytes upon activation of TLR3 with poly (I:C) (Figure 4G). Addition of poly (I:C) nearly doubled the percentage of KRT15-expressing cells and led to a 5-fold increase in number of cells expressing CD200, as assessed by fluorescence-activated cell sorting (FACS) (Figure 4H and 4I).Taken together, these data suggest that TLR3 pathway activation maintains keratinocytes in a less differentiated state and induces the expression of genes associated with hair follicle progenitors.

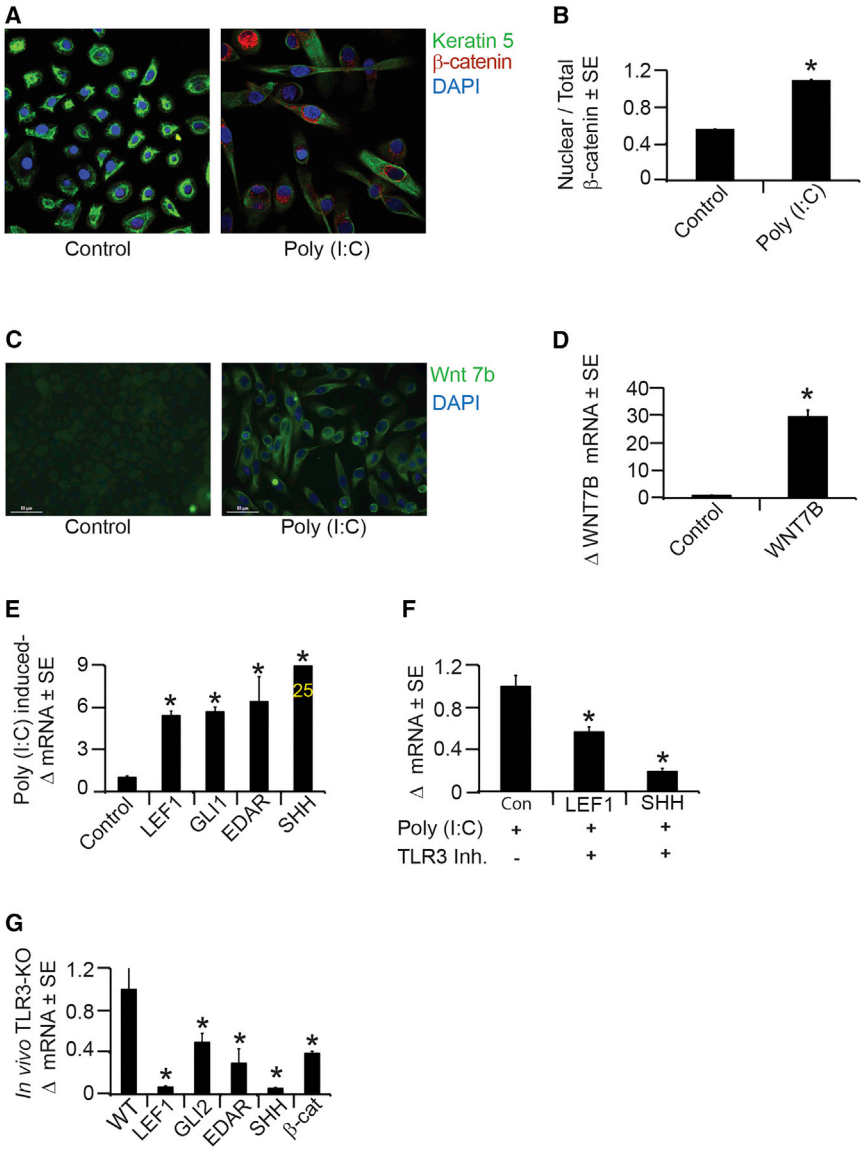

Figure 5. TLR3 Activation Induces Hair Follicle Morphogenic Program Markers

(A) β-Catenin immunofluorescence staining in NHEK after 72 hr of 24 hr treatment with poly (I:C) (20 μg/ml) or control.

(B) Quantitation of nuclear β-catenin to total levels of β-catenin in NHEK as in (A).

(C) WNT7b immunofluorescence staining (green) after 7 days of continuous poly (I:C) (20 mg/ml) or vehicle control treatment to NHEK. Scale bar represents 50 μm; original magnification is 40×.

(D) Mean fold change in *Wnt7b* mRNA after 6 days of continuous exposure to poly (I:C) (20 mg/ml) determined by qRT-PCR and normalized to housekeeping gene, RPLP0.

(E) Mean fold change in *LEF1*, *GLI1*, *SHH*, and *EDAR* mRNA after poly (I:C) treatment by qRT-PCR as in (A).

(F) Mean fold change in *LEF1* and *SHH* mRNA with TLR3-specific inhibitor or control in the presence of poly (I:C) in NHEK as determined by qRT-PCR as in (A).

(G) Mean fold change in *Lef1*, *Edar*, *Gli2*, *Shh*, and *β-catenin* mRNA in TLR3 KO mouse wounds compared with strain-matched control mice as determined by qRT-PCR.

*p < 0.05 by Student's t test or single factor ANOVA.

Hair Follicle Morphogenetic Pathways Are Induced by TLR3 Signaling

We investigated whether these TLR3 activated keratinocytes—with their increased expression of hair progenitor markers—would be poised for subsequent activation of the hair follicle morphogenetic program. Core to this program are the Shh and Wnt pathways, which are activated during both embryonic hair follicle formation and in regeneration following wounding (Ito et al., 2007). First, we examined β-catenin translocation to the nucleus, one of the earliest events in canonical Wnt signaling (Barker, 2008). TLR3 activation with poly (I:C) induced peri-nuclear accumulation and also doubled the amount of nuclear β-catenin in keratinocytes, consistent with activation of the Wnt pathway (Figures 5A and 5B). In addition, expression of the Wnt ligand, Wnt 7b, and the downstream Wnt effector/target gene, LEF1, were upregulated following poly (I:C) treatment of keratinocytes (Figures 5C–5E) (Barker and Clevers, 2010; Tadeu and Horsley, 2014). Similarly, expression of Shh pathway components SHH and GLI1 was increased following poly (I:C) addition, as was the expression of EDAR, another gene active in skin appendage formation (Figure 5E). These pathways were stably induced for several days despite a transient 24-hr treatment of keratinocytes with poly (I:C), suggesting that TLR3 activation may prime keratinocytes toward a hair follicle or appendage fate. Importantly, the pathway activation we observed is TLR3 dependent, as pretreatment of cells with a specific TLR3 small molecule antagonist markedly reduced the expression of both LEF1 and SHH (Figure 5F). A similar dependence on TLR3 was observed in vivo where TLR3 KO mice had decreased expression of β-catenin, Lef1, Gli2, Shh, and Edar following wounding when compared with strain-matched controls (Figure 5G).

Finally, we explored a mechanism by which TLR3 pathway activation promotes induction of the hair morphogenetic program. Expression of *β-catenin* and *GLI2* mRNA was significantly increased in keratinocytes upon poly (I:C) addition (Figure 6A). Since our data demonstrated that stimulation of TLR3 promotes STAT3 activation, we examined whether STAT3 binding sites are present in the promoters of these Wnt and Shh pathway genes. We identified several consensus binding sites. Next, using ChIP-qPCR, we demonstrated a significant increase in STAT3 occupancy at sites in both the β-catenin and GLI2 promoters upon poly (I:C) treatment in keratinocytes (Figures 6B and 6C). These data suggest that TLR3 pathway activation during wounding may lead to direct transcriptional activation of genes involved in hair follicle morphogenesis.

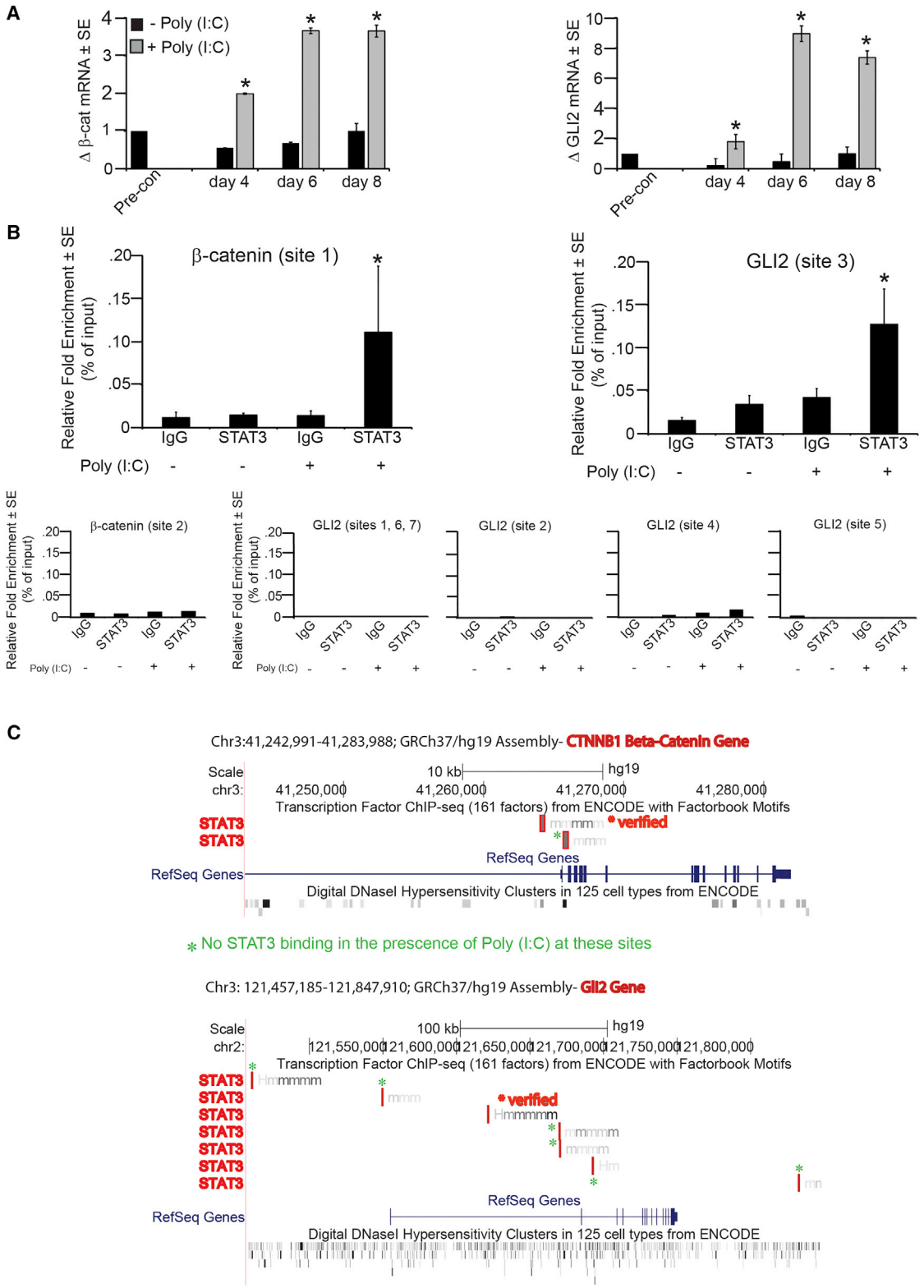

Figure 6. TLR3 Activation Increases STAT3 Occupancy of β-Catenin and GLI2 Promoters

(A) Mean fold change in *β-catenin* and *GLI2* mRNA after continuous exposure to poly (I:C) at indicated time points as determined by qRT-PCR and normalized to housekeeping gene, RPLP0. Fold changes in mRNA expression relative to pre-confluent keratinocytes.

(legend continued on next page)

DISCUSSION

dsRNAs Are Damage-Associated Signals that Promote Regeneration

While a capacity for regeneration is observed in representatives of almost all animal phyla, its distribution is far from uniform, with some species demonstrating regeneration of multiple body parts while closely related species fail to do so (Brockes et al., 2001). Urodele salamanders, for example, are well known to regenerate their limbs, yet among 24 urodele species examined, 4 failed to reconstitute limbs after amputation (Brockes et al., 2001). Even within a single species, differences in genetic background can lead to marked differences in regenerative ability. We and others found that the capacity to regenerate skin and hair follicles, a process termed WIHN, varies greatly among different strains of *Mus musculus* (Figure 1) (Ito et al., 2007; Nelson et al., 2013). While large variation between strains is challenging and requires very careful strain-matched and transgenic controls for all experiments, it is also an opportunity to explore the causes of this biological variation. We harnessed this variation and examined early time points following wounding to search for early, pivotal events that link tissue damage to regeneration.

For regeneration to occur, three interrelated events must take place: (1) organisms must sense loss of tissue integrity, (2) precursor cells must be mobilized to reconstitute missing structures, and (3) these cells must be directed along appropriate morphogenetic pathways (Brockes et al., 2001). While the latter two processes have been extensively examined in studies of regeneration, less is known about how organisms sense damage and transduce this information to trigger a regenerative response. In hydra, the peptide head activator (HA) is secreted at sites of tissue damage and is required for regeneration (Sánchez Alvarado, 2006). In salamanders and newts, an unidentified, thrombin-activated serum factor initiates regeneration of both the limb and lens (Brockes et al., 2001; Imokawa and Brockes, 2003). No such triggers had been discovered in the rare examples of mammalian epimorphic regeneration.

In the context of WIHN, we identified dsRNA released by damaged cells as early molecular signals triggering regeneration. Several lines of evidence support this: dsRNA responsive pathways are upregulated in mice with a high capacity for regeneration, addition of exogenous dsRNA increases the number of regenerated follicles, and degradation of endogenous dsRNA inhibits regeneration (Figure 1). In previous work, dsRNA was shown to be released upon UV-induced damage to keratinocytes (Bernard et al., 2012). Further, dsRNAs have been shown to accelerate re-epithelialization in small wounds of both mice and humans (Lin et al., 2012), suggesting that they play an important, early role in the response to cutaneous wounding. Also, TLR3 has been shown to increase proinflammatory cytokine accumulation after wounding in a manner counterbalanced by cutaneous microflora (Lai et al., 2009). While these studies demonstrate that the dsRNA-TLR3 pathway is active early in wound healing, but its consequences for events after wound closure have not been examined. Our results demonstrate that dsRNA initiates key events in the regeneration process following re-epithelialization.

A major receptor for dsRNA in mammalian cells is TLR3. While originally identified for its role in dorsal-ventral patterning in *Drosophila* and its response to viral pathogens, recent evidence has emerged that TLR3 plays a role in cutaneous wound healing. TLR3-defeicient animals have a decreased inflammatory response to wounding (Lai et al., 2009; Lebre et al., 2007). TLR3 is activated by mRNAs released from dying cells, linking its activation to tissue damage (Karikó et al., 2004). We find that TLR3 is activated in response to cutaneous wounding in mice as *TLR3* mRNA is strongly induced, an effect that can be augmented by administration of exogenous dsRNA. Downstream TLR3 pathway components, including IL-6, are also strongly induced by dsRNA. The activation of IL-6 is critical as it can rescue the defects in hair regeneration observed in TLR3-deficient animals. The early and strong induction of TLR3 and its pathway components upon wounding, coupled with the role of dsRNA in stimulating hair follicle neogenesis, suggest that TLR3 may relay information about tissue damage to activate regeneration. Of note, healed wounds of TLR3 KO mice also have significantly fewer $\gamma\delta$ T cells than WT mice (Figure S5A). These cells have been demonstrated to augment WIHN (Gay et al., 2013), although we find WIHN does occur in mice lacking T and B cells, suggesting that they are not absolutely necessary (Figure S5B). Intriguingly, downstream events induced by TLR3—including possibly recruitment of $\gamma\delta$ T cells—appear to differ between humans and mice (Lundberg et al., 2007). It will be interesting to examine whether differences in TLR3 responses account for the greater regeneration of skin wounds in mice compared with humans.

TLR3 Activation Increases Markers of Hair Follicle Progenitors

In response to damage, organisms must recruit precursor cells to rebuild lost structures. During both physiologic hair cycling and WIHN, KRT15 expressing stem cells of the bulge are mobilized and differentiate into multiple constituent cells of hair follicles. However, during WIHN, cells of the interfollicular epidermis, including those expressing Lgr5 and Lgr6, also contribute to regenerated hair follicles (Ito et al., 2007; Snippert et al., 2010; Tadeu and Horsley, 2014). We find an increase in markers of both types of hair progenitor cells upon activation of the TLR3 pathway. In keratinocytes isolated form interfollicular skin, we observed induction of Lgr6 and KRT15 following TLR3 pathway activation with dsRNA.

These results are in accord with recent findings on the roles of TLR3 and the IL6/pSTAT3 axis in hair follicle and stem cell biology. For example, the induction of hair follicle progenitor markers by TLR3 that we observe is consistent with the correlation of increased KRT15-positive hair follicle stem cells to keratinocyte pSTAT3 during aging (Doles et al., 2012); this and

(B) Relative fold enrichment of STAT3 occupation of β-catenin and GLI2 promoter sites after poly (I:C) treatment of keratinocytes. Negative binding sites are also included below. Data are representative of five independent experiments, $p < 0.05$.

(C) Graphical representation of verified positive and negative STAT3 binding on β-catenin and GLI2 after poly (I:C) treatment of keratinocytes. Images were obtained from the ENCODE database.

*$p < 0.05$ by Student's t test or single factor ANOVA.

another report of drug inhibition of JAK activity promoting anagen might instead be through inhibition of hematopoietic cells (Xing et al., 2014). In further support for our findings, TLR3 has been implicated in the reprogramming of fibroblasts to IPS cells using virally encoded reprogramming factors (Lee et al., 2012). Activation of TLR3 by dsRNA during wounding may similarly promote the conversion of keratinocytes destined to form stratified epidermis into cells with increased capacity for hair morphogenesis.

TLR3 Activation Initiates Hair Morphogenesis

The final event in regeneration is the reactivation of embryonic morphogenetic programs to direct mobilized stem cells to form missing structures. Hair follicle morphogenesis in the developing embryo proceeds through epithelial-mesenchymal crosstalk between the undifferentiated epithelium and the underlying dermis. Our data provide the first physiologic role for TLR3 in Wnt and Shh pathway activation during regeneration, likely through promoting this crosstalk. As with Wnt and Shh signaling, we find that EDAR pathway components are also activated in response to TLR3 signaling in vitro and in vivo. Activation of these appendage specification signals by dsRNA is TLR3 dependent since TLR3 chemical inhibition in vitro or TLR3 gene deletion in vivo blunt the Wnt and Shh pathway. Finally, the IL-6/STAT3 axis directly links TLR3, and these pathways since dsRNA increases occupancy of STAT3 at the promoters of β-Catenin and Gli2. Given the importance in hair development of in vivo epithelial-mesenchymal crosstalk to amplify EDAR, Wnt, and Shh signaling (Millar, 2002), it is notable that we can detect induction of these pathways with keratinocytes alone. We hypothesize these signals will be enhanced in the presence of competent fibroblasts. These findings for TLR3 initiating morphogenesis are consistent with the original description of Toll receptors as regulators of dorsal ventral patterning in *Drosophila* (Anderson et al., 1985). Together with our findings, this suggests that Toll receptors have an equally important role in tissue specification in addition to their more well-known roles in innate immune activation.

In summary, we identified the activation of TLR3 by damage induced dsRNA as the linchpin of the regenerative response to murine skin wounds. Current methods where damage induces rejuvenation (laser resurfacing, dermabrasion, chemical peels) might work through similar mechanisms in humans. Strikingly, TLR3 plays a role in all three aspects of regeneration—damage sensing, precursor recruitment, and activation of hair follicle morphogenesis. As such, TLR3 agonists may be powerful therapeutics to decrease fibrosis and promote cutaneous regeneration.

EXPERIMENTAL PROCEDURES

WIHN

All animal protocols are approved by the Johns Hopkins University Animal Care and Use Committee. C57BL/6J, B6;129SF2/J, TLR3 null mice (B6;129S1-Tlr3$^{tm1Flv/J}$ and B6N.129S1-Tlr3tm1Flv/J), Nod-Scid-Gamma (NOD.Cg-*Prkdc*^{scid} *Il2rg*^{tm1Wjl}/SzJ), and IL-6Rα$^{fl/fl}$ (B6;SJL-*Il6ra*$^{tm1.1Drew}$/J) were obtained from The Jackson Laboratory. K5-Ert2-Cre and K14-Ert2-Cre mice were provided by Pierre Chambon. Stat3$^{fl/fl}$ mice were kindly provided by Cynthia Sears (Johns Hopkins University; Stat3^{tm2Aki}; Takeda et al., 1998), and mixed-strain (C57BL/6J × FVB/N × SJL/J) animals were provided by Dr. Jean Richa (University of Pennsylvania).

A 1-cm^2 excisional full-thickness wound to the level of skeletal muscle on the backs of 21-day-old male and female mice was performed as previously described (Ito et al., 2007; Nelson et al., 2013). Numbers of regenerated hair follicles were quantified in the re-epithelialized skin by non-invasive CSLM, as published (Fan et al., 2011). For all experiments, 50 μl of "intervention" was injected into healing wound (under scab) or applied topically into open wound as shown in the Table 1.

Cell Culture

Neo-natal human epidermal keratinocytes (Lonza) or lab-isolated foreskin keratinocytes were cultured in keratinocyte medium with added supplements (KGM-GOLD). Treatment with recombinant IL-6 protein (50 ng/ml), cucurbitacin I (10–100 nM), poly (I:C) (20 μg/ml), and TLR3 pharmacological inhibitor (80 μM; EMD Millipore) was applied in basal medium containing transferrin, hydrocortisone, and antibiotics for up to 24 hr. After 24 hr, treatment medium was replaced with KGM-GOLD and isolation of RNA as indicated. In some experiments, poly (I:C) was applied for up to a week, with replenishment of poly (I:C) and medium every other day.

Nucleofection

Nucleofection with siGENOME SMARTpool Human TLR3, REL-A, and siCONTROL siRNA duplex oligonucleotides (Dharmacon-ThermoFischer Scientific) was performed in NHEK using the Amaxa 4D-Nucleofector according to manufacturer's instruction. Plated cells were treated with recombinant human IL-6 (50 ng/ml) protein or poly(I:C) (20 μg/ml) for 24 hr. Afterward, treatment medium was removed and replaced with KGM-GOLD complete medium for the duration of the experiment. Levels of appropriate gene expression were assessed by qRT-PCR using inventoried TaqMan reagents in three independent experiments.

Gene Expression Analysis

RNA from immediately re-epithelialized skin at ~12 days after wounding (early stage) or after the earliest time point of hair follicle detection by CSLM (late stage; ~16 days) was submitted to the JHMI Deep Sequencing & Microarray core for Affymetrix Mouse Exon 1.0ST microarray chips according to manufacturer's protocols. Raw gene expression signals in the form of Affymetrix CEL files were extracted and normalized with Partek Genomics Suite software using the Robust Multichip Analysis (RMA) algorithm (Irizarry et al., 2003). The Student's t test ANOVA was used to detect genes with significantly different expression. These analyses have been submitted to the GEO database (under GEO: GSE50418 and GEO: GSE50419; http://www.ncbi.nlm.nih.gov/geo/).

qRT-PCR

Mouse skin was harvested prior to wounding and throughout wounding as described (Nelson et al., 2013). RNA was isolated from NHEK with RNeasy Mini Kit (QIAGEN) with DNase I digestion followed by conversion to cDNA using the High Capacity RNA-to-cDNA kit (Life Technologies). qRT-PCR was performed for genes of interest and 18S or ribosomal protein, large P0 (RPLP0) (housekeeping genes) using inventoried TaqMan reagents. Differences in gene expression were assessed by comparative $\Delta\Delta C_T$ values with fold change calculations.

ELISA

IL-6 protein levels were assayed by ELISA (R&D Systems) from non-wounded and wounded skin or healed mouse scars at times indicated. A minimum of three independent mice was used for each time point.

Immunohistochemistry, Immunocytochemistry, and Histology

Immunohistochemistry was performed on formalin-fixed paraffin-embedded mouse skin samples using the avidin-biotin complex method and AEC development (Vector Laboratories). Indicated antibodies were applied overnight. Sections were counterstained with hematoxylin. Images were captured at 40× magnification using a Nikon Optiphot microscope and Nikon Elements F software. Histology was assessed by H&E after IL-6 addition. The epidermal thickness from the basal layer keratinocytes to beginning of stratum corneum

Table 1. Mouse Strain, Genotype, Number, Intervention, and Schedule Used for WIHN Trials

Experiment	Mouse Strain	Number of Mice	Intervention	Day of Intervention	Day of CSLM Assessment
High versus low gene expression–early; high versus low gene expression–late	C57 versus C57 × FVB × SJL C57 × FVB × SJL	4 per strain; 3 per group	none	–	wound closure; ~WD20-24
Standard WIHN versus fringe Cuts	C57BL/6J	14–15 per group	10 cuts per side	WD0	~WD20-24
Exogeneous poly (I:C) addition	C57 × FVB × SJL; B6;129S1-Tlr3$^{tm1Flv/J}$	10–11 per group; 9 per group	500 ng Poly IC injected into wound	WD3	~WD20-24
Rnase III addition	C57 × FVB × SJL	17–19 per group	15 units Rnase III injected into wound	WD3	~WD20-24
WIHN in TLR3 KO	B6;129S1-Tlr3$^{tm1Flv/J}$; B6;129SF2/J	6 per group	none	–	~WD20-24
Exogeneous IL-6 addition	C57BL/6J B6N.129S1-Tlr3$^{tm1Flv/}$J	30 per group; 8–10 per group	25 ng rmIL-6 protein injected into wound 500 ng rmIL-6 protein injected into wound	WD7	~WD20-24
Importance of IL-6Rα	K14-ERT2-Cre × IL-6Ralpha $^{fl/fl}$ (both C57BL/6)	3–6 per group	intraperitoneal tamoxifin every other day	WD5-WD14	~WD20-24
Cucurbitacin I	C57 × FVB × SJL	10–14 per group	2 mg/kg cucurbitacin I injected into wound	WD7	~WD20-24
Importance of Stat3 in WIHN	K5-ERT2-Cre × Stat3 $^{fl/fl}$ (both C57BL/6)	10 per 15 per group	I.P. tamoxifin every other day	WD0-WD14	~WD20-24
Role of T and B cells	NOD.Cg-Prkdc^{scid}Il2rg^{tm1Wjl} (NOD/ShiLt)	5	none	–	~WD20-24

in three locations per healed mouse wound in multiple histology sections was measured by ImageJ software.

Immunocytochemistry was performed on NHEKs plated on plated on collagen-coated coverslips and treated with 20 μg/ml poly (I:C) as above. Fixed cells were incubated with primary antibodies overnight and appropriate Alexa Fluor secondary antibodies and were counterstained using VectaShield DAPI mounting medium (Vector Labs). Slides were imaged at 60× magnification using the Nikon C1si True Spectral Imaging Confocal Laser Scanning Microscope system (Cell Imaging Core Facility, Sidney Kimmel Comprehensive Cancer Center, Johns Hopkins). Cell morphology and beta-catenin nuclear localization were quantified using the CellProfiler image analysis software (http://www.cellprofiler.org) (Carpenter et al., 2006) from confocal images of nuclei.

Flow Cytometry

Keratinocytes and fibroblasts were fixed, permeabilized (BD Cytofix/Cytoperm kit), and stained with antibodies against human vimentin (BD PharMingen clone RV202), KRT15 (Abam clone LHK15) labeled with a chromophore preconjugated to Fab (Zenon mouse IgG labeling kit) or human CD200 (BD Biosciences; 552475). Data were collected on a dual-laser flow cytometer (BD FACSCalibur) followed by FlowJo 10 (TreeStar) software analysis.

To measure TCRγδ expression, healed wounds (~WD20) from WT and TLRKO3 mice were minced and digested at 37°C in a buffer containing RPMI 1640, 1.67 collagenase Wunsch units/ml Liberase TL (Roche Life Sciences), and 0.01% DNase (Sigma-Aldrich) for 75 min. Following digestion, samples were washed and filtered (40 μm) to obtain a single-cell suspension. Cells were stained with propidium iodide (Miltenyi Biotec) and TCRγδ (GL3) antibody (Miltenyi Biotec) followed by analysis with MACSQuant cytometer and FlowJo software.

Chromatin Immunoprecipitation

Poly (I:C)-treated and control keratinocytes were crosslinked in 1% formaldehyde for 10 min, followed by addition of glycine for 5 min to quench unreacted formaldehyde. Cells were processed with EZ-ChIP Kit (Millipore) according to the manufacturer's instructions. Cross-linked protein-DNA complexes were captured with rabbit anti-Stat3 or normal rabbit IgG (sc-482X; sc-2027X, SCBT) antibodies. qRT-PCR was performed to determine the relative abundance of the promoter DNA sequence, associated with Stat3. Primers are detailed in Supplemental Experimental Methods. Primers and graphics were designed based on ENCODE data (UCSC Genome Browser).

Statistical Analysis

Each experiment was repeated with at least three independent litters of animals or keratinocyte cultures. Data were analyzed using Student's t test or ANOVA single factor. Statistical significance was considered at $p < 0.05$.

SUPPLEMENTAL INFORMATION

Supplemental Information includes Supplemental Experimental Procedures and five figures and can be found with this article online at http://dx.doi.org/10.1016/j.stem.2015.07.008.

AUTHOR CONTRIBUTIONS

A.M.N., S.K.R., and L.A.G. designed the studies, analyzed, and interpreted the results and co-wrote the paper. L.S.M. provided assistance in interpreting results and planning experiments. In addition, T.S.R., M.Z.H., A.S.K., A.S.Z., E.C., S.R.R., C.P., D.K., and A.J.W. assisted A.M.N. and S.K.R. in performing laboratory experiments. All members discussed results and helped formulate ongoing conduct of the project.

ACKNOWLEDGMENTS

The authors thank Conover Talbot Jr. (JHU Microarray Core) for assistance with microarray analysis; Lillian Dasko-Vincent, Cell Imaging Core Facility for assistance with immunocytochemistry analysis; and Dr. Pierre Coulombe and his laboratory for critical discussions. The authors thank Pierre Chambon for use of the K14-Ert2-Cre and K5-Ert2-Cre mouse lines. Research reported in this publication was supported by the National Institute of Arthritis and

Musculoskeletal and Skin Diseases, part of the NIH, under Award Number F32AR062932 to A.M.N. and R01AR064297 to L.A.G. This work was also supported by the Department of Defense, Armed Forces Institute of Regenerative Medicine, Extremities Regeneration (AFIRM2-ER11), Northrop Grumman Electronic Systems, and Alliance for Veterans Support, Inc. (Veteran/Amputee Skin Regeneration Program Initiative), as well as the Thomas Provost, MD Young Faculty Development Fund of Johns Hopkins Dermatology to L.A.G. Johns Hopkins is the owner of a patent application with A.M.N. and L.A.G. as inventors on the use of dsRNA and pathway to promote regeneration and hair follicle neogenesis.

Received: August 26, 2014
Revised: May 28, 2015
Accepted: July 14, 2015
Published: August 6, 2015

REFERENCES

Anderson, K.V., Bokla, L., and Nüsslein-Volhard, C. (1985). Establishment of dorsal-ventral polarity in the Drosophila embryo: the induction of polarity by the Toll gene product. Cell *42*, 791–798.

Barker, N. (2008). The canonical Wnt/beta-catenin signalling pathway. Methods Mol. Biol. *468*, 5–15.

Barker, N., and Clevers, H. (2010). Leucine-rich repeat-containing G-protein-coupled receptors as markers of adult stem cells. Gastroenterology *138*, 1681–1696.

Bernard, J.J., Cowing-Zitron, C., Nakatsuji, T., Muehleisen, B., Muto, J., Borkowski, A.W., Martinez, L., Greidinger, E.L., Yu, B.D., and Gallo, R.L. (2012). Ultraviolet radiation damages self noncoding RNA and is detected by TLR3. Nat. Med. *18*, 1286–1290.

Blaskovich, M.A., Sun, J., Cantor, A., Turkson, J., Jove, R., and Sebti, S.M. (2003). Discovery of JSI-124 (cucurbitacin I), a selective Janus kinase/signal transducer and activator of transcription 3 signaling pathway inhibitor with potent antitumor activity against human and murine cancer cells in mice. Cancer Res. *63*, 1270–1279.

Breedis, C. (1954). Regeneration of hair follicles and sebaceous glands from the epithelium of scars in the rabbit. Cancer Res. *14*, 575–579.

Brockes, J.P., Kumar, A., and Velloso, C.P. (2001). Regeneration as an evolutionary variable. J. Anat. *199*, 3–11.

Carpenter, A.E., Jones, T.R., Lamprecht, M.R., Clarke, C., Kang, I.H., Friman, O., Guertin, D.A., Chang, J.H., Lindquist, R.A., Moffat, J., et al. (2006). CellProfiler: image analysis software for identifying and quantifying cell phenotypes. Genome Biol. *7*, R100.

Doles, J., Storer, M., Cozzuto, L., Roma, G., and Keyes, W.M. (2012). Age-associated inflammation inhibits epidermal stem cell function. Genes Dev. *26*, 2144–2153.

Fan, C., Luedtke, M.A., Prouty, S.M., Burrows, M., Kollias, N., and Cotsarelis, G. (2011). Characterization and quantification of wound-induced hair follicle neogenesis using in vivo confocal scanning laser microscopy. Skin Res. Technol. *17*, 387–397.

Galun, E., and Rose-John, S. (2013). The regenerative activity of interleukin-6. Methods Mol. Biol. *982*, 59–77.

Garza, L.A., Yang, C.C., Zhao, T., Blatt, H.B., Lee, M., He, H., Stanton, D.C., Carrasco, L., Spiegel, J.H., Tobias, J.W., and Cotsarelis, G. (2011). Bald scalp in men with androgenetic alopecia retains hair follicle stem cells but lacks CD200-rich and CD34-positive hair follicle progenitor cells. J. Clin. Invest. *121*, 613–622.

Gay, D., Kwon, O., Zhang, Z., Spata, M., Plikus, M.V., Holler, P.D., Ito, M., Yang, Z., Treffeisen, E., Kim, C.D., et al. (2013). Fgf9 from dermal γδ T cells induces hair follicle neogenesis after wounding. Nat. Med. *19*, 916–923.

Heinrich, P.C., Behrmann, I., Haan, S., Hermanns, H.M., Müller-Newen, G., and Schaper, F. (2003). Principles of interleukin (IL)-6-type cytokine signalling and its regulation. Biochem. J. *374*, 1–20.

Imokawa, Y., and Brockes, J.P. (2003). Selective activation of thrombin is a critical determinant for vertebrate lens regeneration. Curr. Biol. *13*, 877–881.

Irizarry, R.A., Bolstad, B.M., Collin, F., Cope, L.M., Hobbs, B., and Speed, T.P. (2003). Summaries of Affymetrix GeneChip probe level data. Nucleic Acids Res. *31*, e15.

Ito, M., Yang, Z., Andl, T., Cui, C., Kim, N., Millar, S.E., and Cotsarelis, G. (2007). Wnt-dependent de novo hair follicle regeneration in adult mouse skin after wounding. Nature *447*, 316–320.

Jia, C. (2011). Advances in the regulation of liver regeneration. Expert Rev. Gastroenterol. Hepatol. *5*, 105–121.

Karikó, K., Ni, H., Capodici, J., Lamphier, M., and Weissman, D. (2004). mRNA is an endogenous ligand for Toll-like receptor 3. J. Biol. Chem. *279*, 12542–12550.

Karim, R., Meyers, C., Backendorf, C., Ludigs, K., Offringa, R., van Ommen, G.J., Melief, C.J., van der Burg, S.H., and Boer, J.M. (2011). Human papillomavirus deregulates the response of a cellular network comprising of chemotactic and proinflammatory genes. PLoS ONE *6*, e17848.

Kligman, A.M., and Strauss, J.S. (1956). The formation of vellus hair follicles from human adult epidermis. J. Invest. Dermatol. *27*, 19–23.

Lai, Y., Di Nardo, A., Nakatsuji, T., Leichtle, A., Yang, Y., Cogen, A.L., Wu, Z.R., Hooper, L.V., Schmidt, R.R., von Aulock, S., et al. (2009). Commensal bacteria regulate Toll-like receptor 3-dependent inflammation after skin injury. Nat. Med. *15*, 1377–1382.

Lebre, M.C., van der Aar, A.M., van Baarsen, L., van Capel, T.M., Schuitemaker, J.H., Kapsenberg, M.L., and de Jong, E.C. (2007). Human keratinocytes express functional Toll-like receptor 3, 4, 5, and 9. J. Invest. Dermatol. *127*, 331–341.

Lee, J., Sayed, N., Hunter, A., Au, K.F., Wong, W.H., Mocarski, E.S., Pera, R.R., Yakubov, E., and Cooke, J.P. (2012). Activation of innate immunity is required for efficient nuclear reprogramming. Cell *151*, 547–558.

Lin, Q., Wang, L., Lin, Y., Liu, X., Ren, X., Wen, S., Du, X., Lu, T., Su, S.Y., Yang, X., et al. (2012). Toll-like receptor 3 ligand polyinosinic:polycytidylic acid promotes wound healing in human and murine skin. J. Invest. Dermatol. *132*, 2085–2092.

Liu, Y., Lyle, S., Yang, Z., and Cotsarelis, G. (2003). Keratin 15 promoter targets putative epithelial stem cells in the hair follicle bulge. J Invest. Dermatol. *121*, 963–968.

Lundberg, A.M., Drexler, S.K., Monaco, C., Williams, L.M., Sacre, S.M., Feldmann, M., and Foxwell, B.M. (2007). Key differences in TLR3/poly I:C signaling and cytokine induction by human primary cells: a phenomenon absent from murine cell systems. Blood *110*, 3245–3252.

Melkamu, T., Kita, H., and O'Grady, S.M. (2013). TLR3 activation evokes IL-6 secretion, autocrine regulation of Stat3 signaling and TLR2 expression in human bronchial epithelial cells. J. Cell Commun. Signal. *7*, 109–118.

Millar, S.E. (2002). Molecular mechanisms regulating hair follicle development. J. Invest. Dermatol. *118*, 216–225.

Myung, P.S., Takeo, M., Ito, M., and Atit, R.P. (2013). Epithelial Wnt ligand secretion is required for adult hair follicle growth and regeneration. J. Invest. Dermatol. *133*, 31–41.

Nelson, A.M., Loy, D.E., Lawson, J.A., Katseff, A.S., Fitzgerald, G.A., and Garza, L.A. (2013). Prostaglandin D2 inhibits wound-induced hair follicle neogenesis through the receptor, Gpr44. J. Invest. Dermatol. *133*, 881–889.

Sánchez Alvarado, A. (2006). Planarian regeneration: its end is its beginning. Cell *124*, 241–245.

Snippert, H.J., Haegebarth, A., Kasper, M., Jaks, V., van Es, J.H., Barker, N., van de Wetering, M., van den Born, M., Begthel, H., Vries, R.G., et al. (2010). Lgr6 marks stem cells in the hair follicle that generate all cell lineages of the skin. Science *327*, 1385–1389.

St-Jacques, B., Dassule, H.R., Karavanova, I., Botchkarev, V.A., Li, J., Danielian, P.S., McMahon, J.A., Lewis, P.M., Paus, R., and McMahon, A.P. (1998). Sonic hedgehog signaling is essential for hair development. Curr. Biol. *8*, 1058–1068.

Tadeu, A.M., and Horsley, V. (2014). Epithelial stem cells in adult skin. Curr. Top. Dev. Biol. *107*, 109–131.

Takeda, K., Kaisho, T., Yoshida, N., Takeda, J., Kishimoto, T., and Akira, S. (1998). Stat3 activation is responsible for IL-6-dependent T cell proliferation

through preventing apoptosis: generation and characterization of T cell-specific Stat3-deficient mice. J. Immunol. *161*, 4652–4660.

Torok, M.A., Gardiner, D.M., Izpisúa-Belmonte, J.C., and Bryant, S.V. (1999). Sonic hedgehog (shh) expression in developing and regenerating axolotl limbs. J. Exp. Zool. *284*, 197–206.

Uematsu, S., and Akira, S. (2007). Toll-like receptors and Type I interferons. J. Biol. Chem. *282*, 15319–15323.

Xing, L., Dai, Z., Jabbari, A., Cerise, J.E., Higgins, C.A., Gong, W., de Jong, A., Harel, S., DeStefano, G.M., Rothman, L., et al. (2014). Alopecia areata is driven by cytotoxic T lymphocytes and is reversed by JAK inhibition. Nat. Med. *20*, 1043–1049.

Yan, C., Grimm, W.A., Garner, W.L., Qin, L., Travis, T., Tan, N., and Han, Y.P. (2010). Epithelial to mesenchymal transition in human skin wound healing is induced by tumor necrosis factor-alpha through bone morphogenic protein-2. Am. J. Pathol. *176*, 2247–2258.

Cell Stem Cell

Supplemental Information

dsRNA Released by Tissue Damage Activates TLR3 to Drive Skin Regeneration

Amanda M. Nelson, Sashank K. Reddy, Tabetha S. Ratliff, M. Zulfiquer Hossain, Adiya S. Katseff, Amadeus S. Zhu, Emily Chang, Sydney R. Resnik, Carly Page, Dongwon Kim, Alexander J. Whittam, Lloyd S. Miller, and Luis A. Garza

Supplemental Figure Legends

Supp. Fig 1: Related to Figure 1; Microarray analysis at wound closure but prior to regeneration indicates TLR3 signaling signature.
A) Microarray analysis was performed on healed scars at the earliest time of wound closure and re-epithelialization, prior to morphogenesis (~WD12) on Low Regenerating (LR) and High Regenerating (HR) strains of mice.
B) 25 Genes of overlap from Fig **1B** between top 200 genes in HR mice and top 200 genes in dsRNA treated keratinocytes from Karim et al. Fold changes and p-values are from mouse array. Genes in bold are associated with dsRNA recognition or induced by interferon, known TLR3 effects.
C) Wound closure and healing were monitored daily in strain-matched control and TLR3 null mice and average day of scab detachment (SD) as an indication of epithelialization; n = 6 mice.
D) Representative image of non-wounded murine skin after control or poly (I:C) injection (500ng/mouse) during telogen showing no change in hair cycle.

Supp. Fig. 2: Related to Figure 2; Gene expression analysis and qRT-PCR verification of gene expression changes on late stage microarrays.
A) Microarray analysis was performed on healed scars at WD16 on three LR and HR mouse scars as indicated.
B) Signaling pathways enriched and selected changed genes in samples with high regeneration.
C) Top 5 genes associated with enriched signaling pathways in **1B**.
D) Selected significantly changed interleukins, chemokines, and cytokines in HR.
E) Top gene ontology "functions" enriched in HR.
F) qRT-PCR verification of microarray gene expression of selected genes: Interleukin 6 (IL-6); interleukin 10 (IL-10), forkhead box protein P3 (Foxp3). Data represent the Mean ± SE of the fold change in gene expression; n = 5-10; *p < 0.05
G) Mean fold change in IL-6 mRNA with RelA-specific or scrambled control siRNA in the presence of poly (I:C) (20μg/mL) in keratinocytes as determined by qRT-PCR and normalized to housekeeping gene, RPLP0.

Supp. Fig 3: Related to Figure 3; P-STAT3 and IL-6 protein expression during wound healing after Poly IC or rmIL-6 treatment.
P-Stat3 and IL-6 immunohistochemistry in healing murine wounds after poly (I:C) treatment at WD3 or rmIL-6 treatment at WD7; Wounds were harvested 24hrs after treatment and representative images are shown. IL-6 and P-Stat3 positivity is increased during early wound healing (WD4) compared to late wound healing (WD8). Scale bar = 50 μm; original magnification: 40X.

Supp. Fig 4: Related to Figure 4; Increased stratification and altered keratinocyte morphology after IL-6 and TLR3 activation in keratinocytes.
A) Cleaved caspase 3 and Ki-67 immunohistochemistry on healed murine wounds after rmIL-6 treatment; representative images are shown. Scale bar = 100μm; original magnification: 20X.
B) Mean fold change in TLR3 mRNA with TLR3-specific siRNA or siCON (control siRNA) 24 hours after poly (I:C) treatment of NHEKs for 24 hours as determined by qRT-PCR and normalized to housekeeping gene, RPLP0. N=3, * p < 0.05.
C) Keratinocyte morphology 72 hours after 24 hours of poly (I:C) (20μg/mL) or control treatment to NHEK as determined immunofluorescence staining with phalloidin (green), pan-cadherin (red) and DAPI (blue). Magnification = 60X.

D) Quantitation of length to width ratio of keratinocyte morphology as in 4C.
E) Vimentin and keratin 5 immunofluorescence staining in NHEK after poly (I:C) or control as in 4C.
F) Mean fold change in VIM mRNA after poly (I:C) (20μg/mL) addition to NHEK for 24 hours at indicated time points as determined by qRT-PCR and normalized to housekeeping gene, RPLP0.
G) Quantification of vimentin expression via flow cytometry in NHEK after poly (I:C) or control as in 4F or normal fibroblasts.
H) Non-directional keratinocyte migration (μm/hr) after vehicle control or poly (I:C) (20μg/mL) continuous exposure for 7 days.
*$p < 0.05$ by Student's T-test or Single Factor ANOVA.

Supp. Fig. 5: Related to Figure 5; TLR3 KO mice have fewer γδT-cells and WIHN is not impacted in NSG mice.
A) Mean percentage of TCRγδ cells in newly healed wounds in wild type and TLR3 KO mice. Representative FlowJo vX dot plots are shown. N= 3-5 mice per genotype; *$p = 0.001$.
B) WIHN is not affected in NOD.Cg-*Prkdc*^{scid} *Il2rg*^{tm1Wjl}/SzJ mice lacking T and B cell lineages. Cross-sectional H&E histology through the middle of healed scar at WD22 in NSG mice, average number of hair follicles =13; n = 5 mice as measured by CSLM. Regenerated hair follicles are marked with arrows. Scale bar = 100 μm. Original objective: 20X.

A

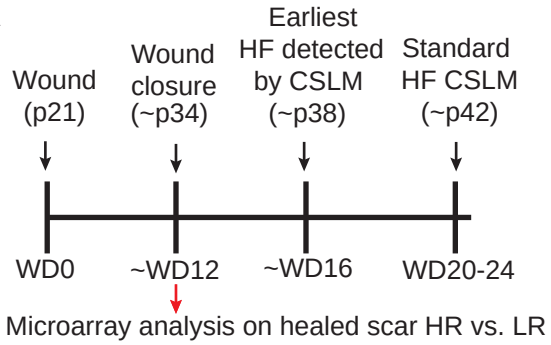

B

Gene Symbol	Gene Name	p-value	Fold Δ	Gene Function
IFIT1	Interferon-Induced Protein With Tetratricopeptide Repeats 1	3.12E-05	3.9194	Interferon induced; anti-viral RNA binding protein
LCE3	Late Cornified Envelope 3	1.27E-02	3.6914	Precursor of cornified envelope
IFI44	Interferon-Induced 44kDa protein	1.81E-05	3.6779	Interferon induced; microtubular structure
OAS1	2',5' Oligosynthetase 1	1.35E-04	2.7335	Innate immune response to viral infection
ISG15	Interferon Stimulated Gene 15	8.24E-05	2.6225	Activated by IFNs; Ubiquitin-like protein; targets RIG-I
IRF7	Interferon Regulatory Factor 7	2.54E-06	2.2975	Innate immune response against DNA/RNA virus
OAS2	2',5' Oligosynthetase 2	1.73E-03	2.2851	Innate immune response to viral infection
CXCL11	Chemokine (C-X-C Motif) Ligand 11	1.36E-04	2.1059	Induced by IFNs, skin immune response
OAS3	2',5' Oligosynthetase 3	1.69E-04	2.0748	Innate immune response to viral infection
RSAD2	Radical S-Adenosyl Methionine Domain Containing 2	1.78E-04	2.0589	Interferon-inducible; anti-viral activity
OASL	2',5' Oligosynthetase-Like	4.49E-04	1.9994	Innate immune response to viral infection
BST2	Bone Marrow Stromal Antigen	7.70E-05	1.9656	IFN-induced anti-viral factor
DHX58	DEXH (Asp-Glu-X-His) Box Polypeptide 58	4.28E-04	1.9042	Regulates DDX58; directly binds dsRNA
DDX58/RIG-I	Retinoic Acid-Inducible Gene 1 Protein	7.15E-04	1.8025	Recognizes dsRNA; innate immune response
PARP14	Poly (ADP-Ribose) Polymerase Family, Member 14	2.36E-04	1.7923	Post-translational modification of histones after DNA damage
XAF1	XIAP Associated Factor 1	3.41E-04	1.7069	Negative regulator of "inhibitor of apoptosis" (XIAP) proteins
HERC6/HERC5	HECT And RLD Domain Containing E3 Ubiquitin Protein Ligase	2.20E-04	1.6458	Ubiquitin ligase
IFI35	Interferon-Induced 35kDa protein	3.86E-05	1.6281	Interferon induced
CXCL9	Chemokine (C-X-C Motif) Ligand 9	7.13E-02	1.6075	T-cell trafficking; immune and inflammatory response
MMP9	Matrix Metalloproteinase 9 (Gelatinase)	4.07E-02	1.6037	Tissue remodeling
CMPK2	Cytidine Monophosphate (UMP-CMP) Kinase 2	4.71E-04	1.5895	Nucleotide synthesis salvage pathway
GBP4	Guanylate Binding Protein 4	2.75E-02	1.3757	Induced by IFNs; hydrolyzes GTP
DEFB103B	Beta-Defensin 3	8.88E-02	1.2254	Antimicrobrial peptide
HELZ2	Helicase With Zinc Finger	3.28E-01	1.1411	Helicase
TRIM5	Tripartite Motif Containing 5	2.75E-04	1.1368	Blocks viral replication

C

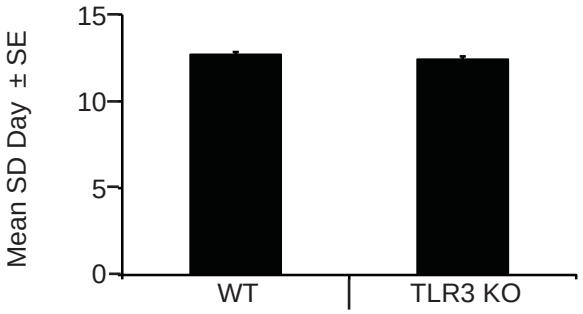

D

A

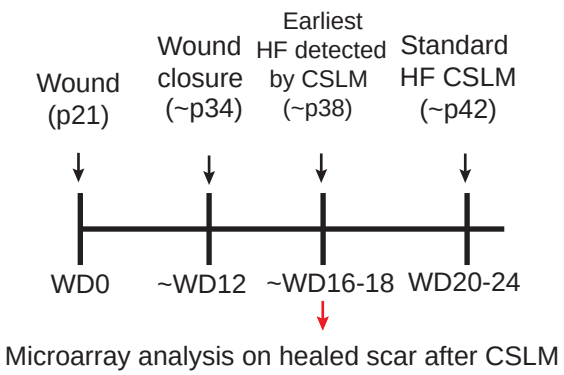

B

Signaling Pathway	P-value
JAK/STAT	***0.0000276***
Corticotropin Releasing Hormone	0.000154
IL-6 Signaling	***0.000212***
IL-10 Signaling	0.000626
Acute Phase Response	***0.000758***

C

Gene Symbol	Fold Δ	P-value
IL-6	3.348	*0.0253*
TNFAIP6	2.518	0.0498
SOCS3	2.183	0.0317
SERPINE1	2.175	0.0141
Fos	2.02	0.000291

D

Gene Symbol	Fold Δ	P-value
Wdr92	6.26	0.0150
Ccl24	***4.23***	***0.0065***
Ptgs2	3.72	0.0042
Il-6	***3.35***	***0.0253***
Nr4a1	2.92	0.0012
Cxcl2	***2.52***	***0.0467***
Cxcl1	***2.10***	***0.0025***
Il-1b	***1.93***	***0.0175***
Ccl3	***1.79***	***0.0186***
Il-10	***1.71***	***0.0341***

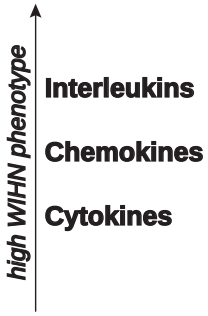

E

GO Bio Function Term	# of genes	P-value
Hematological Function	195	0.00001 < P < 0.01
Inflammatory response	110	0.00001 < P < 0.01
Infection mechanism	105	0.0001 < P < 0.01
Cell-mediated immunity	93	0.00001 < P < 0.01
Organism development	77	0.0001 < P < 0.01

F

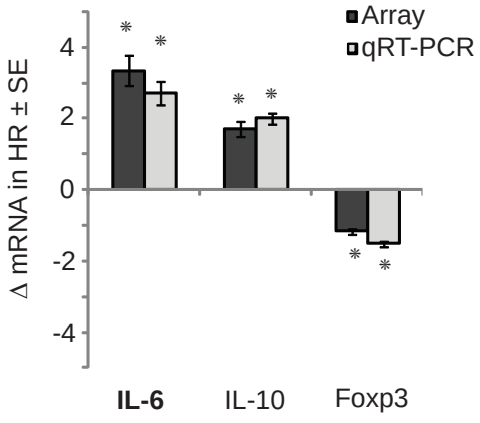

G

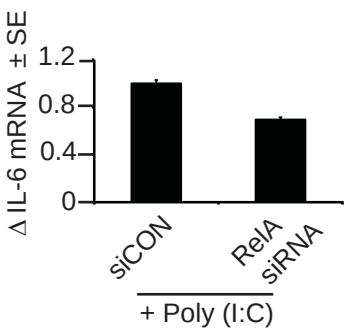

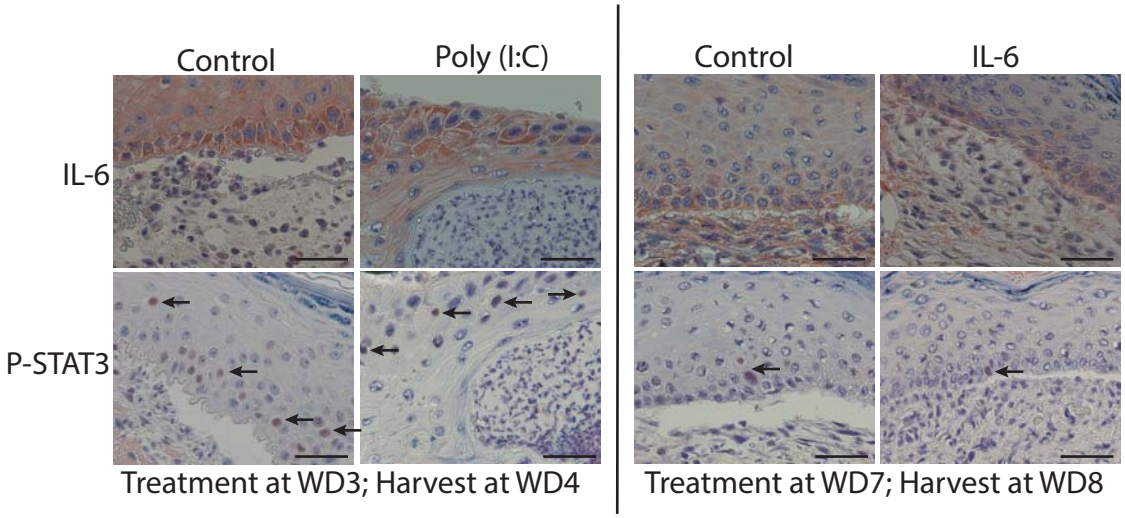
Control
Poly (I:C)
Control
IL-6
IL-6
P-STAT3
Treatment at WD3; Harvest at WD4
Treatment at WD7; Harvest at WD8

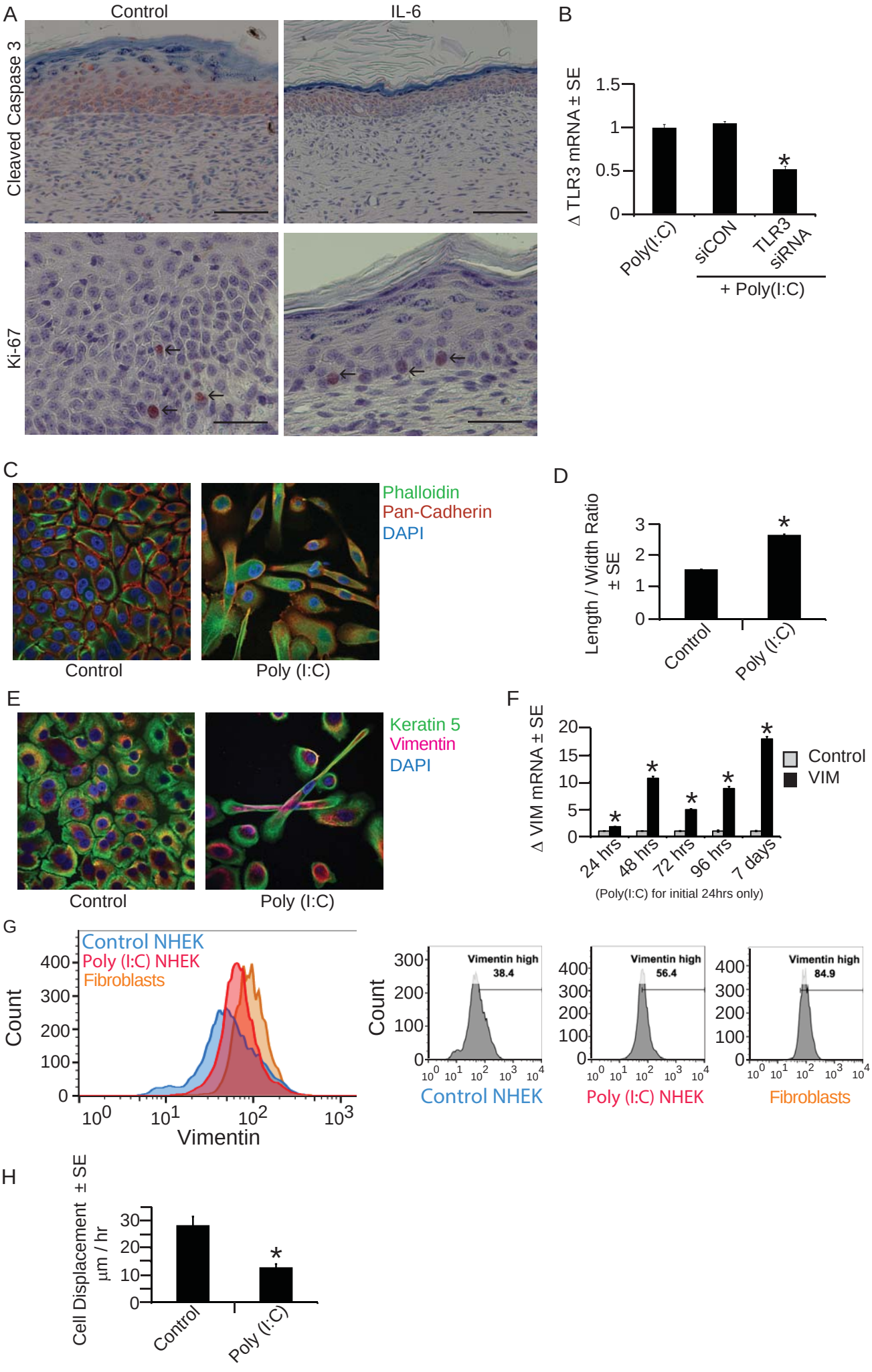
A
Control
IL-6
Cleaved Caspase 3
Ki-67
B
Δ TLR3 mRNA ± SE
1.5
1
0.5
0
*
Poly(I:C)
siCON
TLR3 siRNA
+ Poly(I:C)
C
Phalloidin
Pan-Cadherin
DAPI
Control
Poly (I:C)
D
Length / Width Ratio ± SE
3
2
1
0
*
Control
Poly (I:C)
E
Keratin 5
Vimentin
DAPI
Control
Poly (I:C)
F
Δ VIM mRNA ± SE
20
15
10
5
0
*
Control
VIM
24 hrs
48 hrs
72 hrs
96 hrs
7 days
(Poly(I:C) for initial 24hrs only)
G
Control NHEK
Poly (I:C) NHEK
Fibroblasts
Count
400
300
200
100
0
10^0 10^1 10^2 10^3
Vimentin
Vimentin high
38.4
56.4
84.9
10^0 10^1 10^2 10^3 10^4
Control NHEK
Poly (I:C) NHEK
Fibroblasts
H
Cell Displacement ± SE
μm / hr
30
20
10
0
*
Control
Poly (I:C)

A

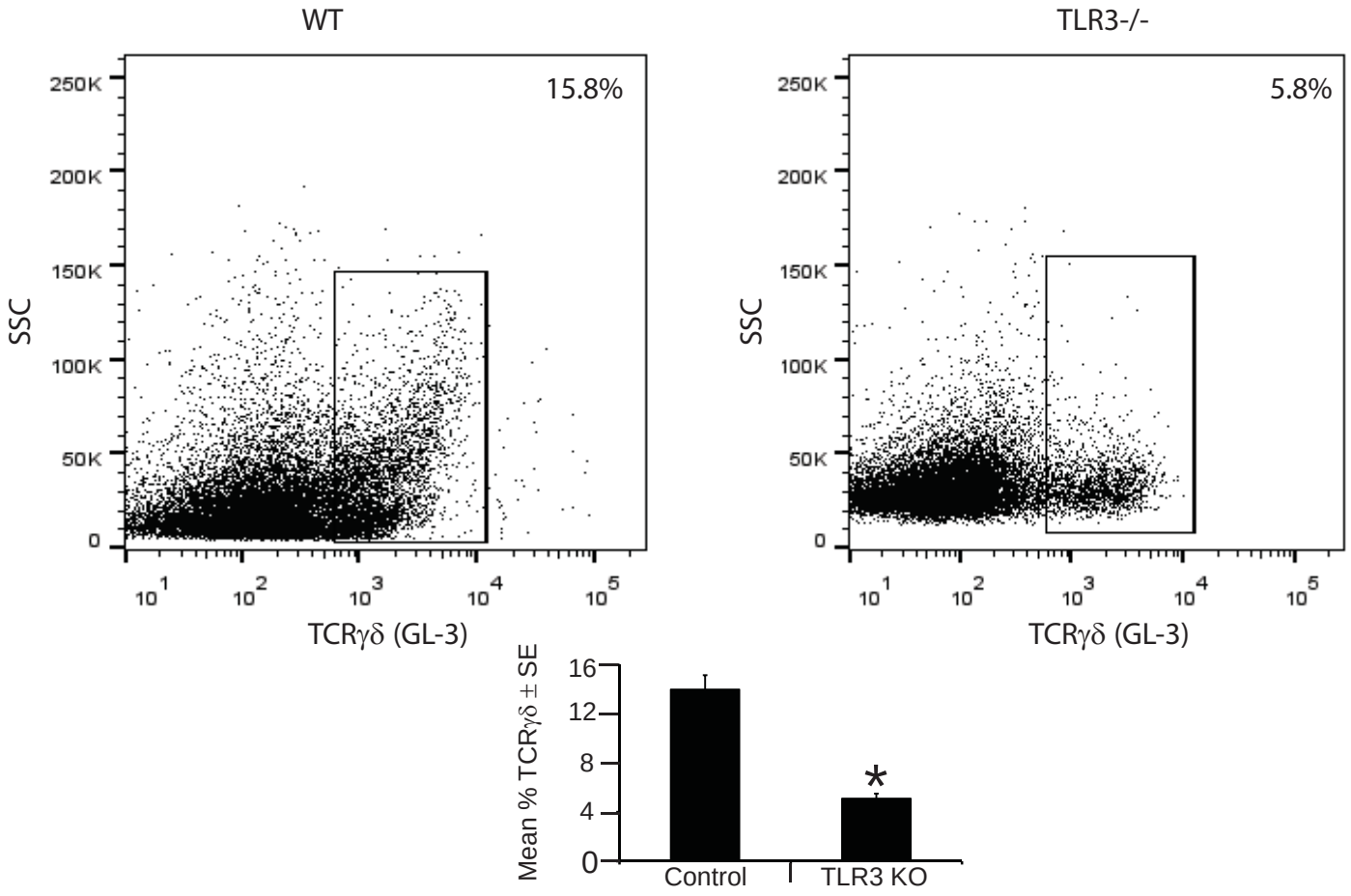

B

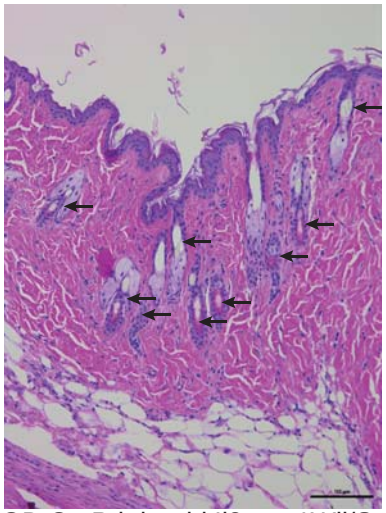

NOD.Cg-Prkdcscid Il2rgtm1Wjl/SzJ

Expanded Experimental Methods

Antibodies

Rabbit polyclonal antibodies to phosphorylated Stat 3, Stat3, Ki-67, cleaved caspase 3, β-actin and secondary anti-rabbit HRP were obtained from Cell Signaling Technology (Danvers, MA). Anti-cytokeratin 1 (Krt1), anti- IL-6, anti- KRT15 (LHK15), anti-Wnt7b (ab94915) and anti-pan-cadherin antibodies was obtained from Abcam (Cambridge, MA). Mouse monoclonal β-catenin antibody (14) and vimentin (RV202) were obtained from BD Biosciences (San Jose, CA) and rabbit polyclonal keratin 5 antibody was purchased from Covance (Princeton, NJ). FITC-Phalloidin was obtained from Sigma (St Louis, MO). Mouse and rabbit IgG isotype controls were purchased from Invitrogen (Camarillo, CA).

Treatments during WIHN assay

Recombinant mouse IL-6 protein (R&D Systems, Minneapolis, MN) and poly (I:C) (High Molecular Weight; InVivogen, San Diego, CA) was diluted in sterile PBS immediately prior to injection. Cucurbitacin I (Tocris Biosciences/R&D Systems, Minneapolis MN) was dissolved in 10% EtOH/PBS to a final concentration of 1mg/mL prior to injection. RNase III enzyme (Life Technologies, Grand Island NY) was diluted in supplied reaction buffer

Keratinocyte Migration Assay

Keratinocytes were seeded onto LabTek II Chambered Coverglass 8-well slides (Thermo, cat. 155409) which had been coated with rat tail collagen I (Gibco, cat: A10483-01). Poly (I:C) was first added (20 ug/ml) 2 days after plating cells (~30% confluent). Subsequently, fresh culture medium (KGM-Gold) and poly (I:C) was applied every other day. At the time of imaging, cells were exposed to poly (I:C) for 7 days. Extended time-lapse imaging was done at the JHU Microscope Facility (acknowledgements: Barbara Smith and Dr. Scot Kuo) for 24 hours inside a humidified, 5% CO2 chamber. Cell migration rate was quantified using SlideBook Reader 6 software (Intelligent Imaging Innovations) by measuring overall cell displacement over the course of one hour (18 cells per video, 3 videos per condition).

ChIP

The amplicon for Gli2 promoter site 4 encompasses TTCCAGGAA on chr2: 121621123-121621782 in the Encode database.
It was amplified with the primer sequences: a) forward: 5'CACAGATAAGCTGAGTCACAGGA3'; b) reverse: 5'TCCTGTTCACATTGACGCC3'. The amplicon for β-catenin promoter site 4 encompasses TTCCTGGAA on chr3: 41264037-41264357 in the Encode database.
This was amplified with the primer sequences: a) forward: 5'TGCCTTTGCATCAACAACAAGG3'; b) reverse: 5'TCAGAAACCAACTGGTCATGTCT3'.